Applied Catalysis B: Environmental 337 (2023) 122987

Contents lists available at ScienceDirect

Applied Catalysis B: Environmental

journal homepage: www.elsevier.com/locate/apcatb

Single atom catalysts for use in the selective production of hydrogen peroxide via two-electron oxygen reduction reaction: Mechanism, activity, and structure optimization

Ke-Yu Chen [b], Yun-Xin Huang [b], Ren-Cun Jin [a,b], Bao-Cheng Huang [a,b,1,*]

[a] School of Engineering, Hangzhou Normal University, Hangzhou 310018, China
[b] School of Life and Environmental Sciences, Hangzhou Normal University, Hangzhou 311121, China

ARTICLE INFO

Keywords:
Single atom catalysts
Two-electron oxygen reduction reaction
Coordinate environment
Active center
Hydrogen peroxide

ABSTRACT

Electrochemically synthesizing H_2O_2 via two-electron oxygen reduction reaction ($2e^-$ ORR) is a promising alternative to substitute the energy-intensive anthraquinone process. In the past years, single-atom catalysts (SACs) have been proposed and widely studied as efficient candidates for catalyzing $2e^-$ ORR, which greatly advances in the H_2O_2 production. Although SACs with different metal centers and coordination structures have been fabricated, the obscure catalytic mechanism impedes their structure design. This critical review summarized the recent progress on $2e^-$ ORR catalyzed by SACs with noble metals, transition metals, and bimetallic as active sites and elaborates on the significance of the binding intensity of *OOH intermediate and active sites in determining the reaction pathway. Additionally, crucial factors including coordination environment, substrate type, and O_2 adsorption configuration that affect SACs performance was discussed. Finally, the structure-performance relationship was unraveled via thoroughly analyzing theoretical justification and experimental findings and future perspectives were envisaged.

1. Introduction

Hydrogen peroxide (H_2O_2) is a valuable chemical with rapidly growing demand in a variety of applications, including chemical synthesis, disinfection, environmental remediation, etc. Currently, industrial-scale synthesis of H_2O_2 is primarily using energy-intensive anthraquinone redox processes [1–3]. However, this multi-step synthesis approach typically requires complex large-scale infrastructure and noble-metal catalysts, while generating large amounts of organic byproducts. The direct synthesis of H_2O_2 from H_2 and O_2 provides a more straightforward alternative that might address the issues related to complex anthraquinone routes [4]. But such a direct synthesis route exposes the potential explosion risk of the hydrogen-oxygen mixture and noble metal catalysts are also required, which increases the cost and presents a big challenge for full-scale application. As a result, exploring efficient and environmentally friendly H_2O_2 production method is still essential [5].

Electrochemically producing H_2O_2, which was proposed by Yamanaka and co-workers [6], through a two-electron oxygen reduction reaction ($2e^-$ ORR) is a desirable technology that may overcome the aforementioned issues [7,8]. In addition, such synthesis process can also be coupled with wastewater remediation technologies such as the electro-Fenton process, where the produced H_2O_2 is directly applied to the subsequent generation of hydroxyl radical [3,7,9]. It is widely accepted that there is a competition between the two- and four-electron pathways for the same intermediate, so a catalyst with a strongly competitive active site to assist the intermediate to following more of the two-electron pathway is needed [10,11]. From this perspective, the design of efficient and cost-effective $2e^-$ ORR electro catalysts to support industrial-scale production of H_2O_2 is warranted.

Noble metals and carbon-based catalysts are the two types of efficient catalysts that researchers have so far fabricated, which showed outstanding selectivity and activity [12–17]. Although a great progress on the above two catalysts has been achieved in the past, there are still some insurmountable limitations [18,19]. Noble metals with low reserves and thereby high price stand as a big challenge for its large scale application. It is preferable to use catalysts devoid of platinum group metals for cost-effective electro-synthesis of H_2O_2 [20–22].

* Corresponding author at: School of Engineering, Hangzhou Normal University, Hangzhou 310018, China.
E-mail address: huangbc@hznu.edu.cn (B.-C. Huang).
[1] ORCID: 0000-0001-7074-4089

https://doi.org/10.1016/j.apcatb.2023.122987
Received 19 March 2023; Received in revised form 28 May 2023; Accepted 9 June 2023
Available online 12 June 2023

Carbon-based materials are advantages in their large surface area, low price, strong conductivity, and superior selectivity [23]. More significantly, the 2e$^-$ ORR activity of carbon catalyst can be further improved through heteroatom doping strategy. However, a large over-potential that occurs throughout the reaction process is still significant, which presents as a barrier for carbon-based catalysts [24].

Tuning active centers and evaluating catalyst activity at the atomic scale have become possible due to advances in synthesis, calculation, and characterization techniques, pushing the catalytic community further into the era of single atom catalysts (SACs) [25]. Compared to nanoscale catalysts, SACs successfully attained the objective of expanding atomically active sites. Metal atoms are segregated and fixed by coordinated atoms to form a single active site [26], which results in a theoretically maximum 100% atomic utilization and performs with a high stability and activity [27]. By selecting porous and high surface area material such as carbon as substrate, the prepared SACs may possess the benefits of both metal and carbon materials to provide high mass transfer efficiency and high selectivity [23,28]. The actual catalytic activity of a SACs material is vulnerably affected by several factors including geometric effect, as well as the coordination environment and substrate carrier. Getting in-depth understanding on how the above factors influence the intermediate formation and catalytic selectivity is fundamental for SACs based 2e$^-$ ORR catalyst design and application. Benefiting from the significant advances in cutting-edge computational techniques development, our knowledge on catalytic mechanism of 2e$^-$ ORR by SACs has been greatly expanded in the past years. Herein, it is essential to summarize the state-of-art and future challenges of SACs for catalyzing 2e$^-$ ORR, to better facilitate its industrial application.

This review intends to conduct a comprehensive evaluation on the research status quo of catalyzing 2e$^-$ ORR by SACs. The catalytic mechanism and reaction thermodynamic of ORR on SACs were introduced, via combining with latest advances on the density functional theory (DFT) calculation. The development of noble metal, transition metal, and diatomic SACs catalysts in controlling the activity and selectivity of 2e$^-$ ORR was summarized. Potential influences of several key factors, including coordination environment, carrier type, and geometric structure, on SACs activity were discussed. The structure-performance relationship between the SACs configuration and their electrocatalytic activity and selectivity was unraveled through analyzing theoretical justification and experimental findings. Also, the SACs stability issue during its long-term use was discussed. At last, future prospects for the design and application of SACs based 2e$^-$ ORR catalyst is outlooked.

2. The mechanism and thermodynamics of producing H_2O_2 via 2e$^-$ ORR

The activity and selectivity of oxygen reduction process are largely governed by the interaction of intermediates with the active center, which can be reflected by its adsorption energy [29]. In order to rationally design SACs with optimum selectivity and catalytic activity, it is essential to understand how ORR works on SACs. Herein, a typical SACs structure with N coordinated metal on a carbon substrate was adopted to discuss its reaction mechanism (Fig. 1a) [30]. Unlike the conventional bulk or nanoscale catalyst (such as Pt nanoparticles [31]) that owns continuous active sites, the intermediate and SACs during ORR are linked to avoid O-O bond cleavage (Fig. 1b). Recognizing ORR from the ground up is necessary if one intends to influence it further in the desired direction [2]. ORR either goes along 2e$^-$ pathway via stabilizing the intermediate to produce H_2O_2, or breaks the O-O bond of the intermediate to produce H_2O, as shown in Fig. 1c [32]. Hence, the activity and selectivity of the ORR depend heavily on how the intermediate interacts with the catalyst and how energy is converted [33,34]. Fully understanding of the structure-activity relationship between active sites and intermediate adsorption energy is a prerequisite for rational design of catalysts. In addition, increasing the catalyst's mass transfer efficiency, applying reasonable electrode potentials, and modifying the electrolyte's pH are also helpful to improve the reaction's selectivity [2,35,36].

It is generally accepted that the generation of H_2O_2 through 2e$^-$ ORR involves two electrons transfer and one reaction intermediate, while the four-electron reaction pathway consists of four primitive steps and three different reaction intermediates:

$$O_2 + (H^+ + e^-) \rightarrow *OOH + (H^+ + e^-) \rightarrow H_2O_2 \quad (1)$$

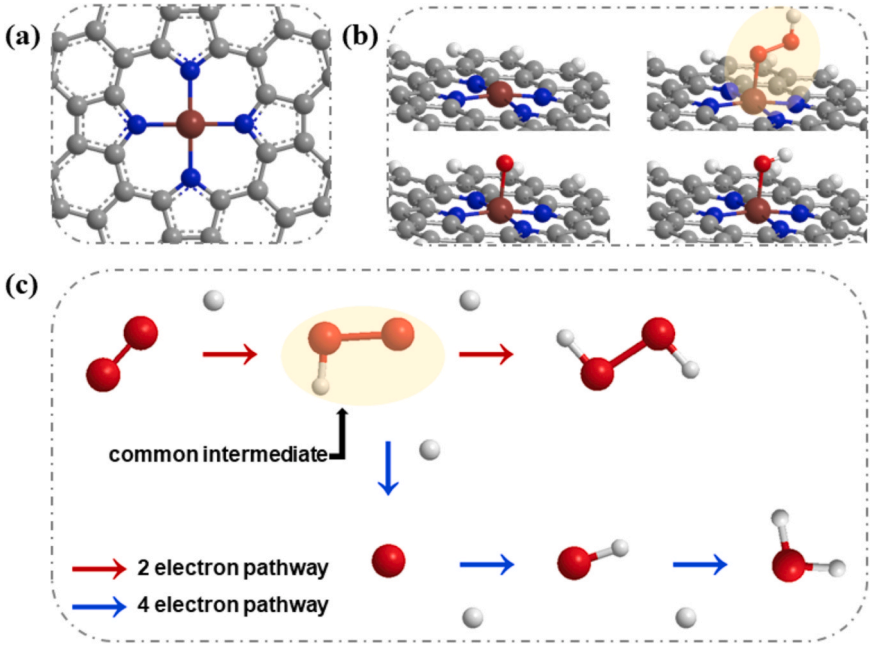

Fig. 1. (a) Schematic diagram of single atom catalysts molecular model. (b) The most suitable structures of *OOH, *O, and *OH adsorbed on M atom in single atom catalysts. (c) The ORR process via 2e$^-$ and 4e$^-$ pathway in acidic media. (white ball, H; blue ball, N; black ball, C; red ball, O; dark red ball, metal, including Mn, Fe, Cu, Ni, Co, etc.).

$$O_2 + 4(H^+ + e^-) \rightarrow *OOH + 3(H^+ + e^-) \rightarrow *O + 2(H^+ + e^-) \rightarrow *OH + (H^+ + e^-) \rightarrow H_2O \quad (2)$$

where * denotes an unoccupied active site, and *OOH denotes the single adsorbed intermediate for the reaction. Table 1 shows the standard electrode potentials for reducing several intermediates, and it can be seen that H_2O has a higher standard electrode potential and is more easily generated during oxygen reduction with a thermodynamic advantage [37]. In the course of the ORR, there is a clear competition between the 4e⁻ and 2e⁻ pathways [38]. Fig. 1b shows the three intermediates adsorbed on SACs. From the Eqs. 1 and 2, it can be noted that *OOH is the common intermediate between the two ORR pathways and the binding strength between the catalyst and the *OOH intermediate determines the reaction product.

The 2e⁻ ORR tends to proceed more stably in an acidic environment due to its unique characteristics. In acidic electrolytes, catalytic reaction begins with O_2 molecules adhering to the active site and protons and electrons react to form *OOH intermediates (Eq. 1), which are then converted to H_2O_2 or broken down to form *O intermediates (Eq. 2) [2]. The choice of pH environment, however, cannot be generalized and must consider the downstream circumstances of usage. The behavior of the proton during ORR, namely its ability and selectivity to bind which O atom of *OOH intermediate, influences the selectivity of the subsequent ORR and is also related to the pH dependence [16,39]. The 2e⁻ and 4e⁻ pathways compete with one another, as illustrated in Fig. 2a. In order to optimize H_2O_2 production, SACs applied to 2e⁻ ORR must be liable to O_2 adsorption and *OOH desorption while against *OOH dissociation. The catalyst which is affinity to the 2e⁻ product prevents the synthesis of H_2O since it is a thermodynamically advantageous product [40]. Preventing the dissociation of the O-O bond in *OOH is essential for avoiding the 4e⁻ pathway, hence a catalyst that promotes *O production is not appropriate for 2e⁻ ORR [41]. Even though we have these crucial details, the ambiguity of the active center and the unpredictability of the structure-performance relationship make it difficult to advance the catalyst's development.

The challenge of quantitatively determining the adsorption energy between the reaction intermediate and the catalyst structure can be resolved, thanks to the advancement of modern spectroscopic equipment and computational simulation [42]. The screening and design of active sites that may have high activity and selectivity can be realized using DFT calculations [43]. The structure-performance relationship at the atomic scale can be discovered via combing theoretical computations with experimental study. By utilizing this research paradigm, it helps designing materials enriched with more efficient active sites and forecasting whether the catalyst will work well.

Nørskov et al [44] first built a typical catalytic process calculation approach for evaluating the stability of the intermediate based on the computed hydrogen electrode model and simulated adsorption energy [11,45]. The proton and electron pair used in the model has a chemical potential that is equivalent to that of the proton and electron pair in hydrogen gas at $U = 0$ V. By transferring the electron energy $-eU$, where e and U are the basic charge and electrode potential, respectively, the impact of electrode potential on the free energy of the reaction intermediate is taken into consideration. As shown in Fig. 2b, the dotted line refers to the standard equilibrium potential of 2e⁻ ORR and 4e⁻ ORR. The peak value of the volcano gram represents the highest activity (highest limit potential and lowest over-potential) that can be attained in each pathway. The shaded region represents the selective region of H_2O (blue) or H_2O_2 (green) products. It is worth noting that the *OH and *OOH intermediates follow a scaling relationship [46]. The adsorption energies of *OH and *OOH can be used as descriptors of 2e⁻ and 4e⁻ ORR activities. The free energy diagram for the 2e⁻ ORR at a standard potential of 0.70 V is shown in Fig. 2c [13]. Under maximal activity, the free energy of an ideal catalyst is flat at 0.70 V, resulting in a zero over-potential. The intermediate will develop vertically if the active site is too strong to combining with it, which may prevent the reaction from preceding at 0.70 V. The overall process demands excessive energy expenditure when the thermodynamic over-potential is too high, and the reaction cannot continue normally. A well-performed catalyst will have a high current density at a small over-potential since it is at the volcano diagram's peak and its free energy diagram is flat at equilibrium potential.

In order to show more intuitively how to choose a suitable catalyst, the limiting potential of the 2e⁻ ORR can be represented by *OOH as a descriptor based on the scalar relationship between the different descriptors, corresponding to $\Delta G_{*OOH} = \Delta G_{*OH} + 3.2$ and $\Delta G_{*O} = 2\Delta G_{*OH}$, as shown in Eqs. 3 and 4.

$$U_{L1} = -\Delta G_{*OOH} + 4.92 \quad (3)$$

$$U_{L2} = \Delta G_{*OOH} - 3.52 \quad (4)$$

Fig. 2d shows the calculated 2e⁻ volcano diagram between the limiting potential and ΔG_{*OOH} for each step through Eq. 3 (red line) and Eq. 4 (black line) [43,47]. The lowest limiting potential of the fully catalytic reaction is indicated by the intersecting black and red solid lines, which corresponds to an equilibrium potential of 0.70 V. Therefore, in principle, it is possible to design an electrochemical catalyst with ideal activity around the volcano peak, where the *OOH binds to the catalyst at an appropriate strength. For catalysts with a strong *OOH bonding energy located on the left side of the 2e⁻ volcano (black solid line), *OH → H_2O will become the potential rate-determining step and the 4e⁻ ORR may dominate. On the other hand, in the case of weak *OOH binding on the right side of the volcano (red solid line), O_2 → *OOH is the potential rate-determining step, which is expected to increase the H_2O_2 selectivity but decrease the activity. As a result, the most desirable catalyst with high activity and selectivity for H_2O_2 synthesis is likely to be found at the top of the 2e⁻ volcano diagram. Overall, DFT can be used as an advanced screening approach to accurately identify catalysts that satisfy both catalytic activity and selectivity requirements, and provide a theoretical foundation for preparing a workable catalyst.

Table 1
Standard electrode potentials for ORR half reactions in acidic and alkaline electrolyte [37].

ORR pathway	Electrolyte	Half reactions	E^0 (V *vs.* RHE)
4e⁻ pathway	Acid	$O_2 + 4H^+ + 4e^- \rightarrow 2H_2O$	1.229
	Alkaline	$O_2 + 2H_2O + 4e^- \rightarrow 4OH^-$	0.401
2e⁻ pathway	Acid	$O_2 + 2H^+ + 2e^- \rightarrow H_2O_2$	0.695
		$H_2O_2 + 2H^+ + 2e^- \rightarrow 2H_2O$	1.763
	Alkaline	$O_2 + H_2O + 2e^- \rightarrow HO_2^- + OH^-$	-0.065
		$HO_2^- + H_2O + 2e^- \rightarrow 3OH^-$	0.867

3. Performance on catalyzing 2e⁻ ORR by SACs

To address the activity, selectivity, and stability issues, the electronic structure, physiochemical structure, and active sites of a 2e⁻ ORR electrocatalyst should be well tuned. However, due to the irresistible adsorption of reaction intermediates, adjustment of the intensity of bound *O for H_2O_2 production is usually accompanied by a change in *OOH adsorption energy, leading to a decrease in selectivity. Herein, the tradeoff between high activity and selectivity still remains a great challenge. The coordination environment and substrate types of SACs can significantly influence the electronic structure of individual atoms, which can be well tuned to enhance their reactivity with oxygen molecule and create a suitable bonding strength with intermediates for achieving an improved 2e⁻ ORR selectivity [48,49]. Currently, different types of SACs have been successfully fabricated and applied for electro-synthesize of H_2O_2 (Table 2).

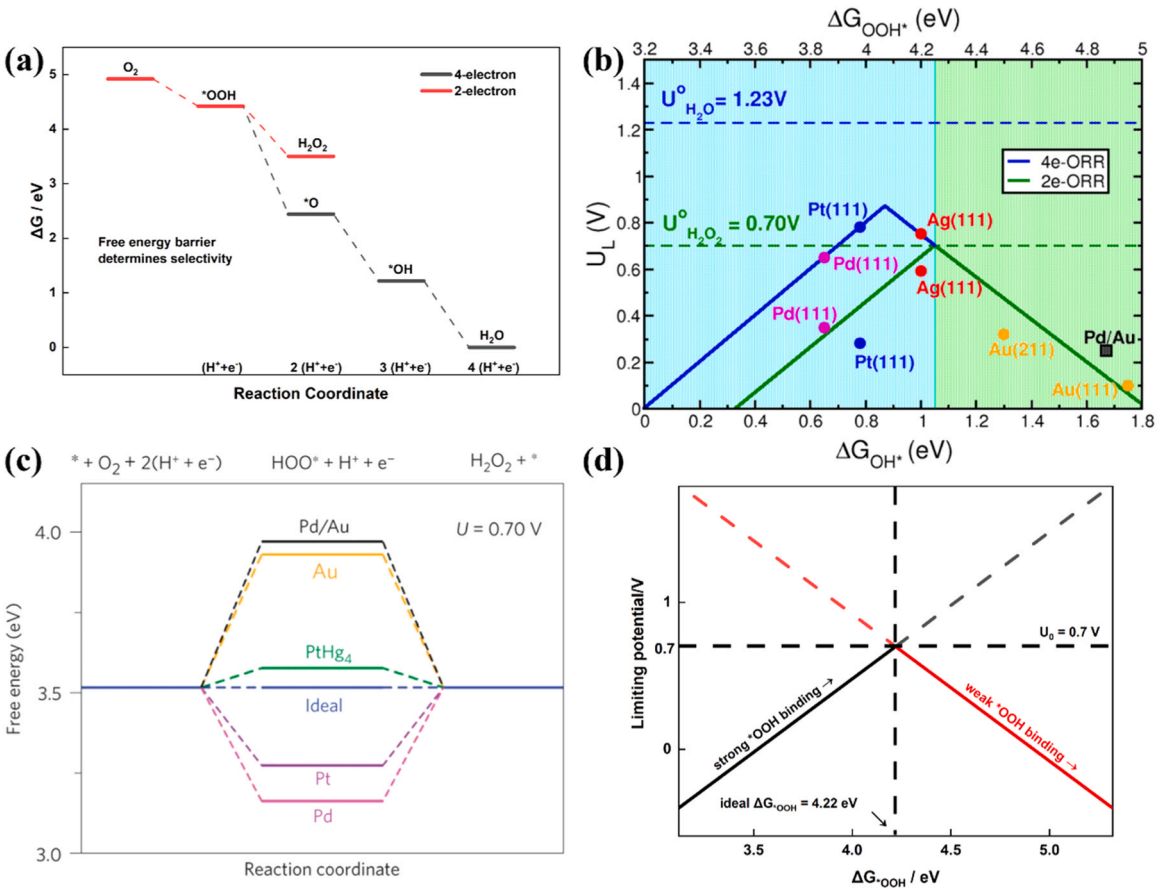

Fig. 2. (a) Free energy diagram for the 4e⁻ (black line) and 2e⁻ (red line) oxygen reduction. (b) 2e⁻ ORR (green) and 4e⁻ ORR (blue) activity volcano plots including the activity of noble transition metals. Shaded blue and green areas represent the regions with high selectivity for H_2O and H_2O_2, respectively. (c) Free energy diagram for the 2e⁻ ORR at 0.70 V. (d) Limiting potentials for individual steps in Equations (3) and (4), showing the strongly bound *OOH region (solid black line) and weakly bound *OOH region (solid red line) for the 2e⁻ pathway.
(a) Adapted with permission from [40]. Copyright 2018 AmericanChemical Society. (b-c) Adapted with permission from [13]. Copyright 2013Macmillan Publishers Limited.

Table 2
The electrochemical catalytic performance of single atom catalysts.

Electrocatalysts	Metal content (*wt.*%)	Electrolyte	E_{onset} (V *vs.* RHE)	J_k (mA cm^{-2})	Selectivity (%)	Activity (mg L^{-1} h^{-1} mg$^{-1}_{cat.}$)	Ref.
Pt_1-meso-S-C	—	0.1 M $HClO_4$	0.855	10 at 0.6 V	87	24.01	[22]
Pt-N-CNT	0.04	0.1 M $HClO_4$	0.62	—	72.5	> 275	[60]
Pt1/N-C	0.3	0.1 M $HClO_4$	0.57	12.5 at 0.3 V	> 80	—	[136]
Co-N-C	2.65	0.1 M $HClO_4$	0.69	0.57 at 0.1 V	> 70	23.39	[72]
Mn-N-C	1.52	0.1 M $HClO_4$	0.57	0.56 at 0.1 V	> 70	—	[72]
Co_1/NC	0.9	0.1 M $HClO_4$	0.75	32	80	20.60	[70]
Co-N SAC_{Dp}	0.84	0.1 M $HClO_4$	0.632	14.4 at 0.5 V	94	26.7	[67]
Rh_1/NC	0.89	0.1 M acetate buffer 0.1 M KCl	0.68	—	100	370.91	[55]
O-Co-N_2C_2	0.74	0.1 M PBS	0.72	2.48 at 0.5 V	> 90	121.38	[73]
CoPc-OCNT	0.3	0.1 M K_2SO_4	0.75	0.94 at 0.4 V	> 95	132.33	[43]
Co-N_2-C/HO	0.88	0.1 M KOH	0.801	11.3 at 0.6 V	91.3	1000	[96]
ZnNC	—	0.1 M KOH	0.78	2.4 at 0.2 V	84	—	[65]
ZnO_3C	0.7	0.1 M KOH	0.78	2.9 at 0.2 V	> 80	11.9	[86]
$N_4Ni_1O_2$/OCNTs	0.1	1 M KOH	0.68	350 at 0.65 V	82.1	193.8	[97]
FeNi-C-N	8.61	0.1 M KOH	0.699	3.153	100	—	[82]
Mo_1/OSG-H	> 10	0.1 M KOH	0.78	2.78 at 0.3 V	95	—	[88]
In SAs/NSBC	0.97	0.1 M KOH	0.66	1.12 at 0.5 V	95	220.66	[87]
W_1/NO-C	1.7	0.1 M KOH	0.815	2.56 at 0.5 V	> 90	41.82	[99]

3.1. Noble metal SACs

Several highly active catalysts have been developed to improve ORR performance via the 4e⁻ pathway, but there are not so many catalysts available for selectively reducing O_2 to H_2O_2. Noble metals and its alloys such as Pt [50], Pt-Hg [51], Pd-Au [11], Pd-Hg [13], and Au-Pt-Ni [14] are currently viewed as effective catalysts with a low over-potential and high H_2O_2 selectivity. The synthesis of active metal nanoparticles has reportedly attained the size and active sites close to that of single atoms, according to several studies [51,52]. However, compared with active metal nanoparticles, isolated active metal atoms normally exhibit a higher selectivity for H_2O_2 production (Table 3). The active metal atom

Table 3
Performance of nanoparticle catalysts and SACs on 2e⁻ ORR.

Electrocatalysts	Metal content (*wt.*%)	E_{onset} (V *vs.* RHE)	J_k (mA cm^{-2})	Selectivity (%)	electron-transfer number (n)	Ref.
Ni-NP/G	20	0.94	2.21 at 0.6 V	25	3.5–3.7	[53]
Ni-SA/G	1.5	0.79	4.42 at 0.6 V	~94	~2	
Co_{NP}-N-C	0.23	0.7	2.9 at 0.1 V	~30	3.5	[54]
Co_{SA}-N-CNTS	0.79	0.7	3.4 at 0.1 V	~95	~2	
Pt-NP/rGO	5	0.964	0.94 at 0.3 V	~30	3.5–3.6	[50]
Pt-SA/rGO	0.5	0.764	7.05 at 0.3 V	~95	2–2.3	
Pt/TiC	5	0.68	3.03 at 0.2 V	24.8	3.4	[56]
Pt1/TiC	0.2	0.47	0.96 at 0.2 V	68	2.4	
Pd/C	20	0.94	5.7 at 0.2 V	~0	~4	[62]
C@C_3N_4-Pd_1	0.5	0.67	3.2 at 0.2 V	94	~2	

was demonstrated to be segregated by other inert elements in each alloy, and this tactic is in line with both geometric effects and the SACs design ethos [53–55].

Although Pt is known to be a 4e⁻ ORR catalyst, its selectivity can be shifted to the 2e⁻ pathway when it is dispersed at the atomic level. Song et al [50] synthesized Pt-SA/rGO with Pt loading of 0.5 *wt.*% via a simple impregnation method. The reduction peak of Pt-SA/rGO located at 0.813 V *vs.* RHE, which is more positive than those of Pt nanoparticles (Pt-NP/rGO) and Pt clusters (Pt-CT/rGO), indicating that highly dispersed Pt atoms can enhance the reaction efficiency by fully exposing the metal sites. The atomic-scale dispersion property provides opportunities to alter the reaction pathways of ORR. It could be observed that the J_R of Pt-SA/rGO is significantly enhanced and the corresponding H_2O_2 selectivity could reach up to 95%, which was significantly higher than that of Pt nanoparticles (Figs. 3a and 3b). Meanwhile, the electron transfer number of Pt-NP/rGO is closest to 4 while that of Pt-SA/rGO is closest to 2. Another similar study also showed that altering Pt based catalyst from nano-scale to atomic-scale dispersion, the H_2O_2 selectivity could be greatly improved from 24.8% to 68.0% [56]. Herein, tuning catalyst size into atomic-scale is effective to shift ORR pathway from 4e⁻ to 2e⁻. In addition, increasing the number of active sites can also improve the selectivity and activity performance of the electrocatalyst [57,58]. One approach is to construct hollow nanosphere structures by dispersing Pt atom on amorphous CuS_x support with single-atom Pt sites up to 24.8 *at.*% [59]. The high ring current of Pt_1-CuS_x in an acidic electrolyte, as determined using the rotating ring-disk electrode (RRDE), indicates its good selectivity for H_2O_2 (92%−96%). Meanwhile, Pt_1-CuS_x exhibits high activity and stability over a wide potential range of 0.05–0.7 V *vs.* RHE. However, sometimes too much metal loading can be a burden for SACs. Zhao et al [60] explored the effect of isolated Pt site density on ORR pathway regulation by preparing Pt-N-CNT with different Pt loadings. The TEM characterization of the catalysts revealed that with the increase of Pt precursor addition, partial Pt single atoms would aggregate to form Pt nanoparticles inside the catalysts when the Pt loading exceeded 7 *wt.*%, but overall, it was still consistent with the characteristic of highly dispersed Pt sites (Fig. 3c). They plotted the

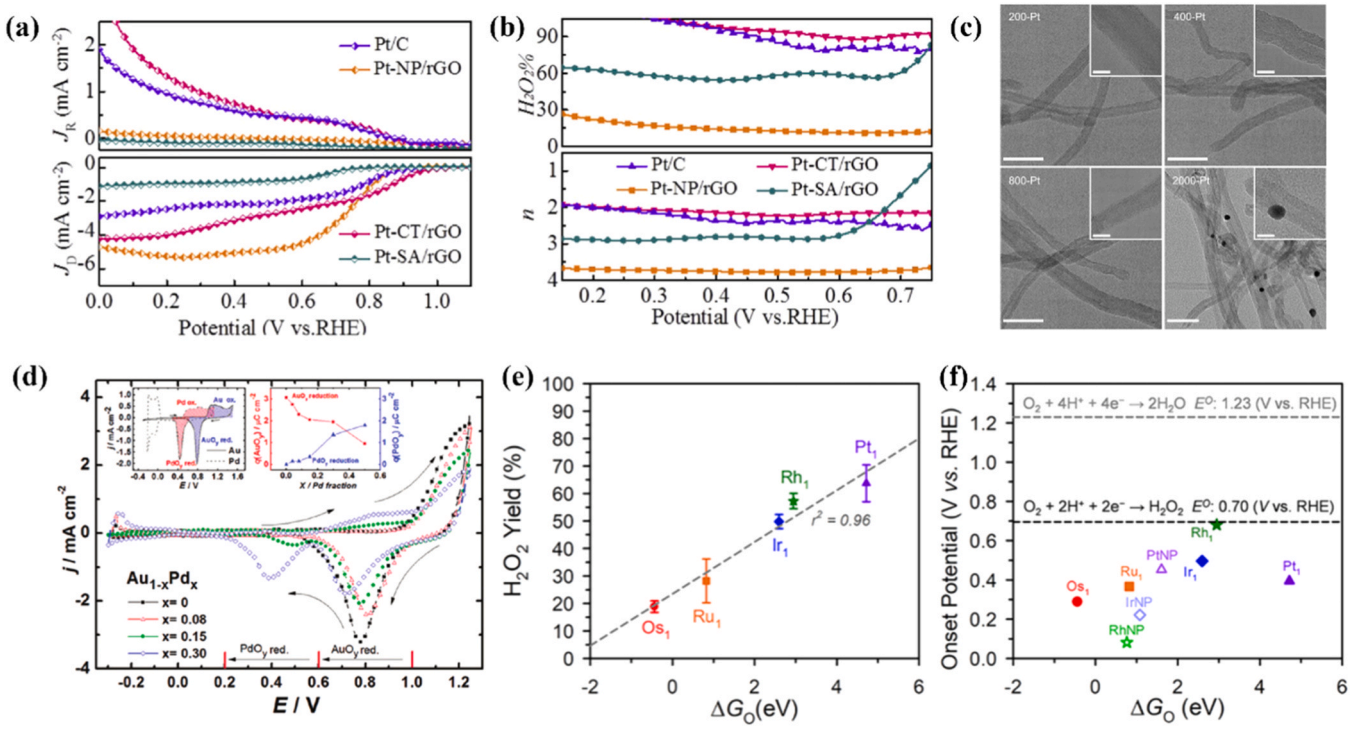

Fig. 3. (a) Rotating Ring-Disk Electrodes curves of Pt-SA/rGO, Pt-CT/rGO, Pt-NP/rGO, and Pt/C catalysts. (b) electron-transfer number (n) and H_2O_2 selectivity (H_2O_2%) of Pt-SA/rGO, Pt-CT/rGO, Pt-NP/rGO, and Pt/C catalysts. (c) TEM images of 200-, 400-, 800- and 2000-Pt-N-CNT. (d) Cyclic voltammetry (CV) curves of $Au_{1-x}Pd_x$/C nanoalloysin Ar saturated 0.1 M $HClO_4$. (e) Linear relationship between the DFT-calculated ΔG_O values and the experimentally determined H_2O_2 yields of the atomically dispersed catalysts. (f) Volcano-shaped relationshipbetween the O binding energies and the onset potentials for the 2e⁻ ORR pathway for M_1 and MNP catalysts.

(a-b) Adapted with permission from [50]. Copyright 2019 Elsevier. (c) Adapted with permission from [60]. Copyright 2022 Nature Publishing Group. (d) Adapted with permission from [51]. Copyright 2011 American Chemical Society. (e-f) Adapted with permission from [64]. Copyright 2020 American Chemical Society.

correlation between Pt site density and H_2O_2 selectivity. The H_2O_2 selectivity plummeted (from 70% to 20%) with increasing Pt site density, indicating a shift of the ORR pathway from the $2e^-$ to $4e^-$ pathway. It is evident that the selection of appropriate metal loading is crucial to improve the H_2O_2 selectivity.

Au and Pd SACs are also verified as efficient $2e^-$ ORR catalysts. Jirkovsk et al [51] screened appropriate metals to fabricate electrocatalysts, by following the research paradigm of theoretical prediction and experimental test. They showed that Au SACs modified with scattered Pd had better catalytic performance than pure gold. Under 8% molar Pd concentration, a notable improvement in oxygen reduction selectivity for H_2O_2 generation close to 95%, was achieved. However, further increasing Pd content would result in a decline in catalytic activity and the H_2O_2 selectivity decreased to less than 10% at 50% Pd concentration (Fig. 3d). Scattering single atom Pd on porous carrier such as hollow titanosilicate nanospheres [61] or C@C_3N_4 [62] is another efficient approach to improve the H_2O_2 selectivity. Compared to monatomic Pt, Pd appears a lower energy requirement for generation of H_2O_2, thereby showing a higher selectivity [62]. Other studies compared various forms of O_2 adsorption on Pd and discovered that O-O bond breaking on Pd atoms was significantly inhibited [57,63]. Furthermore, O_2 was more readily activated to form *OOH while H_2O_2 dissociation was inhibited, resulting in higher activity and selectivity. For comparing the correlation between noble metal types and ORR pathway, Joo et al [64] prepared five atomically dispersed noble metal catalysts (Os, Ru, Rh, Ir, and Pt) by the "trapping-and-immobilizing" method. It was found that Pt-CNT showed the highest H_2O_2 selectivity (≈95%) in 0.1 M $HClO_4$, while Rh-CNT showed the best activity. The trend of H_2O_2 selectivity is shown in Fig. 3e, fitted by DFT calculation, which shows a proportional increase in H_2O_2 selectivity as the *O binding energy diminishes. For the $2e^-$pathway, Rh_1 is located at the top of the volcano plot, although its selectivity is slightly inferior to that of Pt_1 (Fig. 3f). Experiment and theoretical calculations show that the high selectivity of Pt SAC is attributed to the weaker oxygen binding strength and that the optimal binding energy of Rh SAC is responsible for its high activity. Overall, noble metal-based SACs exhibit higher activity and selectivity compared to nanoparticle catalysts, mainly due to their weaker intermediate binding energy and metal atomic level distribution.

3.2. Transition metal SACs

Transition metal SACs are promising alternatives to precious metals in a wide range of electrocatalytic reactions. Although much efforts have been devoted to improving their activity and stability, there is still a large gap in performance between transition metal SACs and commercial Pt-based catalysts in practical applications, especially under acidic conditions. The preparation of stable and efficient non-precious SACs catalysts still faces many challenges [65]. Recently, researchers have introduced transition metals into the N-doped carbon skeleton to form M-N-C (M denotes metal) single atom structure to stabilize and activate the metal cations [66,67], trying to improve the catalytic performance for $2e^-$ ORR. Among the M-N-C SACs catalysts, Fe-N-C is one of the most widely studied structure and its catalytic mechanism is well investigated. Normally, Fe-N-C materials exhibit a high catalytic activity and selectivity for $4e^-$ ORR, which is consistent with the behavior of Fe-porphyrins and Fe-phthalocyanines [68]. Earlier studies have shown that Co-porphyrins and Co-phthalocyanines usually catalyzed $2e^-$ ORR, with H_2O_2 as the main product [69,70]. Therefore, a better understanding of the catalytic activity and selectivity of M-N-C materials for $2e^-$ ORR seems to be highly advisable.

It is generally accepted that the interaction between the 3*d* orbitals of the central metal and the *p* electrons of the intermediate oxygen species affects the final activity and selectivity of catalyst. Sun et al [23] synthesized a number of M-N-C SACs (M = Fe, Co, Ni, Mn, and Cu) and evaluated their performances of selective production of H_2O_2. Combining DFT calculations and experiments together, they discovered that the highest selectivity of the Co-N-C catalyst for H_2O_2 is justified by its binding free energy to *OH intermediate with values that bring Co-N-C close to the top of the $2e^-$ volcano (Fig. 4a). The calculated activity of Co-N-C is comparable to that of the noble metal alloys reported in earlier studies. Although M-N-C SACs exhibited a promising potential for H_2O_2 production via $2e^-$ ORR in an acidic electrolyte (Fig. 4b) [23,30,71], effective kinetic calculations to explain their intrinsic catalytic performance were still lacking. Shen et al [72] combined experiments and calculations to investigate the catalytic activity trends of M-N-C SACs (M = Co, Fe, Mn). They found that Mn-N-C and Co-N-C exhibited excellent H_2O_2 selectivity of over 70% in the 0.3–0.5 V *vs.* RHE range, while Fe-N-C showed selectivity as low as 35%. As shown in Fig. 4c, combining thermodynamic and kinetic analyses, a descriptor (E_{*H_2O} - E_{*HOOH}) was proposed to illustrate and predict the H_2O_2 selectivity and ORR pathway on the catalyst. Using this descriptor, they successfully predicted and experimentally verified the high H_2O_2 selectivity of Co-N-C [73]. In comparison, Fe-N-C catalyst exhibited a strong binding affinity to *OH, leading to the dominance of $4e^-$ pathway. The above theoretical prediction and experimental verification research paradigm guides the rational design of M-N-C catalysts with high selectivity for H_2O_2 generation. Tian et al [74] also concluded that the spatial distribution of metal center would greatly affect SAC performance. They prepared edge-rich Co-N/HPC catalyst and found that it displayed outstanding $2e^-$ ORR performance throughout a broad potential range, with up to 95% selectivity. The edge host atom Co-N_4 site is discovered to be thermodynamically more advantageous for $2e^-$ ORR than the base plane site. Significantly, the Co-N_4 site at the -OH functionalized zigzag edge (Co-N_4/ZZ-edge-OH), located at the summit of the volcano, had the maximum catalytic activity toward the $2e^-$ ORR and showed zero over-potential (Fig. 4d-e). Moreover, enriching the epoxy group close to the Co-N_4 sites that are hosted by the basal plane can significantly enhance the detachment of *OOH intermediates.

However, the H_2O_2 activity and selectivity of a metal element is not set in stone. Metal single atom anchored on carbon-based materials can be tuned by metal coordination motifs. By flexibly adjusting different transition metal coordination motifs in carbon nanotube (CNT) substrate, Jiang et al [75] discovered that Fe-C-O was a high-efficient H_2O_2 catalyst with an unprecedented on-set potential of 0.822 V, limiting current of 0.1 mA cm^{-2}, and H_2O_2 selectivity above 95% at both basic and neutral pH values. DFT calculations identified that the Fe-C-O motif, in contrast to the well-known Fe-N-C to driving $4e^-$ ORR, was responsible for the H_2O_2 production. Metal single atom prefers to chemically bind to C and O in the CNT vacancy, forming a stable M-C-O structure rather than simply adsorbing to the CNT. When O atoms were doped into the catalyst, the limiting potential of the system was substantially reduced, leading to an over-potential as low as 0.07 V. In addition, it was found that the Fe atoms in the Fe-C-O motif typically enhanced the *OOH binding by C site, indicating the key role of Fe and O atoms in the coordination. Besides that, a number of other transition metals, including Ni, Mn, and Zn as metal active sites of SACs, can also contribute to $2e^-$ ORR [65]. For example, Ni SACs is synthesized by a simple “Schiff base ligand-mediated” pyrolysis strategy [76]. The obtained Ni-N_2O_2/C catalyst exhibited 96% H_2O_2 selectivity, which is higher than that of NiN_4/C catalyst. The reaction mechanism of O_2 on Ni-N_2O_2/C catalyst is similar to that of O_2 on homogeneous Schiff base catalyst. The formation of superoxide intermediate promotes the electrocatalytic reduction of O_2 to H_2O_2. Wei et al [77] prepared Zn SACs with asymmetric structure property via "pre-adsorption-anchoring and pyrolysis" strategy. After structural optimization, the electrocatalyst Z-PPy-600 had ultrahigh Zn loading (up to 11.34 *wt.*%) and exhibited excellent H_2O_2 selectivity up to 90%. In order to investigate the relationship between catalyst structure and activity, they summarized the correlation between Zn loading amount and catalyst performance (Fig. 4f). There was a positive correlation within a certain range of Zn loading but further increasing Zn atom amount would induce a declined catalytic performance, implying

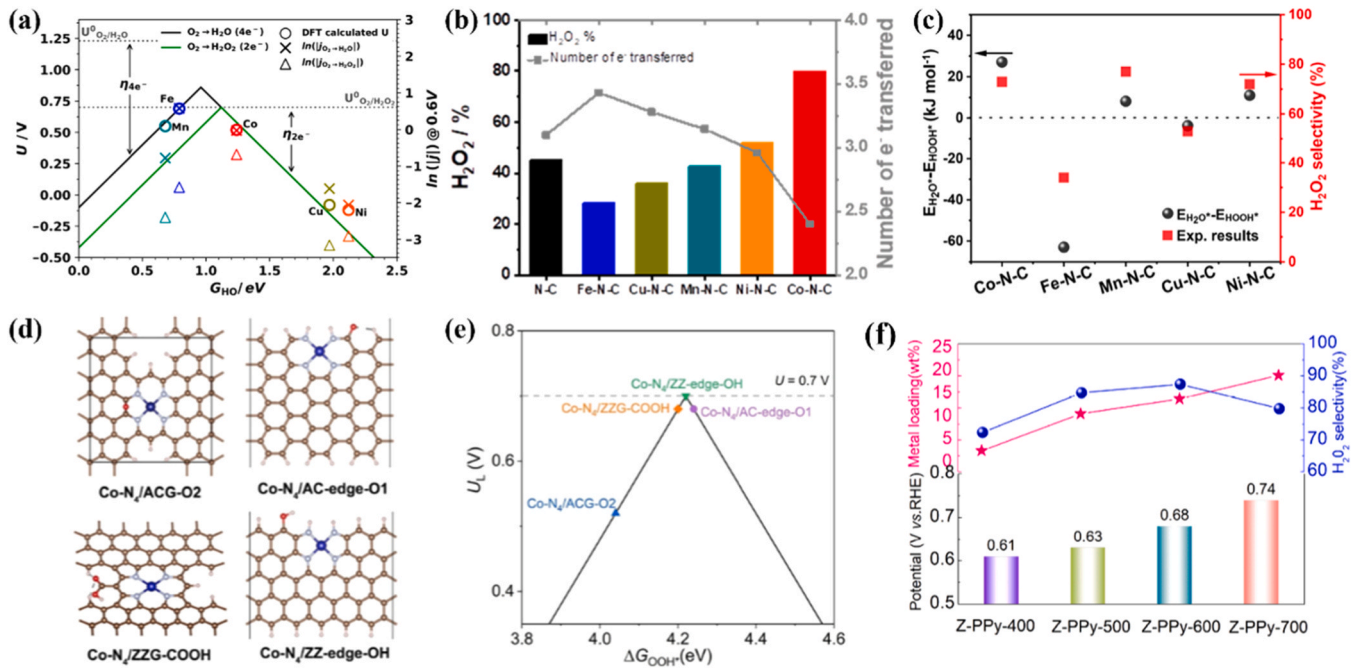

Fig. 4. (a) Thermodynamic relations (volcano) lines for the 2e$^-$ (green solid line) and 4e$^-$ ORR (black solid line). (b) H_2O_2 selectivity and the number of electrons at +0.1 V *vs.* RHE derived from RRDE data. (c) Comparison between the kinetic descriptor (E_{*H2O} - E_{*HOOH}) and the experimentally measured H_2O_2 selectivity for M−N−C (M = Co, Fe, Mn, Cu, and Ni). (d) Optimized structural models of Co-N_4/ACG-O2, Co-N_4/AC-edge-O1, Co-N_4/ZZG-COOH and Co-N_4/ZZ-edge-OH. (e) Corresponding volcano plot for the 2e$^-$ ORR. (f) The histogram of the onset potentials, the curves of calculated average H_2O_2 selectivity and the Zn loading of the Z-PPy-T.

(a-b) Adapted with permission from [23]. Copyright 2019 AmericanChemical Society. (c) Adapted with permission from [72]. Copyright 2022American Chemical Society. (d-e) Adapted with permission from [74]. Copyright2022 Wiley-VCH GmbH. (f) Adapted with permission from [77]. Copyright 2022 Elsevier.

that the single atom loading was not the only factor determining the selectivity. Generally, combining metal types and other modulation methods may open up new opportunities for designing highly efficient transition catalysts for 2e$^-$ ORR.

3.3. Double-metal atom catalysts

Recently, double-metal atom catalysts (DACs) have been proposed as more effective electrocatalysts than SACs [78]. Instead of metal clustering, DACs are constructed on a substrate where two metals interact to form active sites together. By fusing the properties of the alloys, DACs can change the electron density of the single metal active site, modestly adjust the catalytic reaction performance, and prevent the catalyst from forming metal nanoparticles. As an example, Jiang et al [79] used first-principle simulation to design stable dual transition metal ORR catalysts based on C_2N. Comparing to SACs, DACs own a higher adsorption energy to O_2 and lower dissociation barrier of *OOH, which are more efficient and lastingly well performed. O_2 molecule on TM_2@C_2N is in a lateral adsorption configuration, where two O atoms were bonded to two TM atoms and pulled out of the C_2N plane. Compared to SACs, this allows O_2 to gain a more polarized charge from the catalyst and elongates the O-O bond length, implying higher activity and suggesting that the DACs system is easy to dissociate O_2. In general, DACs combine the advantages of alloy catalysts and SACs, and the rational design of their active site structure is feasible to enhance the catalyst performance.

Even though there is still a significant research gap regarding the use of DACs in 2e$^-$ ORR, several pertinent studies undoubtedly showed the outstanding performance and great application promising of DACs. Cao et al [80] investigated the stability of PdCu@C_2N based on molecular dynamics and DFT simulations and the geometrical configuration of the above catalysts revealed that both the bimetallic Ru-Cu and Pd-Cu adopted a similar configuration with one metal atom at the top and the other at the bottom (Fig. 5a-b). O_2 is preferentially adsorbed onto the top atom when it is close to the catalyst surface, avoiding the decomposition of O_2 molecules into two oxygen atoms by the bimetallic atoms, as shown in Figs. 5c and 5d. This is also in line with the requirement of H_2O_2 production, which should maintain the stability of the adsorbed O_2 molecules on the catalyst to avoid O_2 desorption or dissociation. In addition, the introduction of a second metal center allows the interaction between noble and non-noble metals, leading to charge rearrangement on the active sites, which contributes to the performance of the catalyst. For example, Zhang et al [81] synthesized an atom-dispersed Pt-Co catalyst on a nitrogen-doped carbon carrier (A-CoPt-NC). It was showed that electrons were transferred from Pt to Co, which promoted the reduction of O_2 to *OOH and facilitated the *OOH desorption to further generate H_2O_2. In addition, the energy of the Co 3*d* orbital moves up, indicating a stronger binding between the catalyst and O_2, which is consistent with the analysis of charge redistribution.

When the second metal cooperates with the M-N site, unlike the electronic effects caused by heteroatom doping or functional groups, the introduction of the second metal provides multiple adsorption sites and modulates the adsorption strength of the O_2 molecule, thus avoiding the dissociation of the O-O bond. Some advanced 4e$^-$ ORR catalysts, such as FeCo-N-C [34], can achieve high activity and 4e$^-$ ORR selectivity by reducing the O-O bond cleavage potential barrier via synergistic interaction between Fe and Co atoms. Therefore, the rational design of DACs may pave a new way to improve the 2e$^-$ ORR catalytic activity and stability. Setyowati et al [82] obtained transition metal and nitrogen doped carbon catalysts via polymerization and direct pyrolysis and FeNi-C-N showed the highest current density compared to other single metal-based catalysts. The composite bimetal showed a more uniform nitrogen distribution on the surface, as demonstrated by the high specific surface area and pore volume, which enhanced the 2e$^-$ ORR activity. The capacitance value is related to the conductivity of the

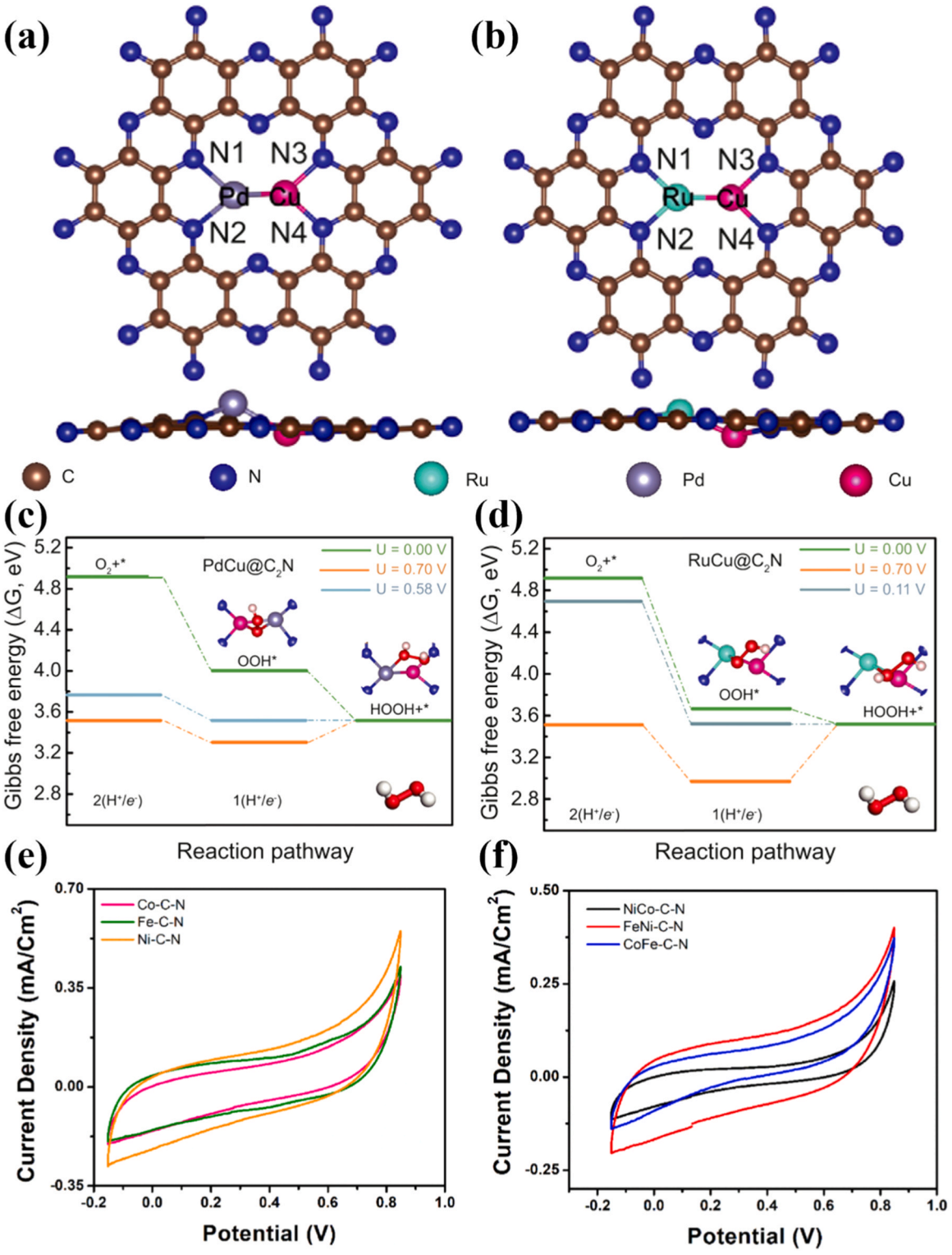

Fig. 5. (a-b) Top and side views of atomic configurations of PdCu@C_2N and RuCu@C_2N. (c-d) Free energy diagrams for the 2e$^-$ ORR mechanisms on RuCu@C_2N and RuCu@C_2N at zero potential (green line), applied potential (blue line), and equilibrium potential (yellow line). (e) CV curves of single precursor-based catalyst. (f) CV curves of dual precursor-based catalyst.
(a-d) Adaptedwith permission from [80]. Copyright 2021 ScienceDirect. (e-f) Adapted withpermission from [82]. Copyright 2022 Elsevier.

material, and high capacitance indicates a material with high conductivity. By scanning cyclic voltammetric curves, it was found that the CoFe-C-N catalyst has lower specific capacitance when Co and Fe are combined, and the catalyst will achieve the best performance when Fe and Ni, two metals that themselves exhibit higher capacitance values in monometallic materials, are synthesized as FeNi-C-N (Fig. 5e-f). It can be seen that the presence of bimetallic active sites might play a synergistic role, thus enhancing the catalyst performance [83].

Many subsequent studies have confirmed that dual-atom catalysts with bimetallic sites have special properties. By constructing dual atom

catalytic centers, both the electronic structure and reaction mechanism of SACs can be regulated, thereby tuning its catalytic activity. Wang et al [84] synthesized a new catalyst ((Fe, Co)/CNT) with Fe-Co double sites embedded in N-doped CNT. DFT calculations indicated that the synergistic effect of Fe-Co double centers is beneficial to weaken the activation of O-O bonds on oxygen, thereby improving the catalytic activity. In addition to using different metals to construct DACs, there are also studies on DACs with the same atoms. Ye et al [85] synthesized Fe_1-N-C, Fe_2-N-C, and Fe_3-N-C structure within one catalyst by high temperature pyrolysis. Fe_1-N-C does not contain Fe-Fe bonds, while double metal sites appear in Fe_2-N-C and Fe_3-N-C. DFT calculations showed that when the bimetallic Fe sites formed, Fe_2-N-C and Fe_3-N-C were favorable for O_2 adsorption, and the extended O-O bond made it easier to activate. In addition, it is also found that Fe_2-N-C had more catalytic centers and stronger bond hybridization between Fe 3*d* and O 2*p* orbitals than that of Fe_3-N-C.

DACs combine the benefits of alloy catalysts and carbon-based materials as one method of controlling the surface geometry of catalysts. The alloy metal is anchored on the carrier through metal-support interaction, which can effectively control the stable coexistence of two active sites and avoid the agglomeration of metal atoms In addition, the two metal sites can participate in the reaction through different mechanisms. For example, the dissociation pathway may be applicable to diatomic catalysts because there are multiple active centers, which is different from SACs [69]. Importantly, if both metal sites are involved in the reaction, the scaling relationship limiting ORR activity can be broken and catalysts with better activity can be prepared.

4. Tuning strategies of improving the catalytic activity and selectivity of SACs

The ORR selectivity and activity of catalysts usually depend on the adsorption behavior of the key intermediate *OOH on the active site, both in terms of intensity and structure. It is strongly influenced by the electronic structure of the catalyst central metal, which is mainly related to the structure of the metal *d*-band center. However, in addition to the electronic structure differences triggered by different central metals, the SACs coordination environment, substrate type, etc. also affect the fine control of the ORR pathway. Electronic structure modulation would inturn change the both configuration and bond length of the central metal with O_2 molecule and intermediates, thus changing the catalytic performance of SACs. Due to the structural heterogeneity and complexity, the exact role of the coordination environment on catalyst performance improvement in a practical catalytic system is complicated. Subsequently, several key factors, including substrate type, ligand atoms and number, and geometric effects, are further discussed to guide more efficient SACs ORR catalyst design.

4.1. Selectivity improvement via coordination environment modification

It is more common to find SACs in the form of M-N-C on carbon substrates. However, the M-O-C motif has a strong ability to alter the intrinsic binding strength of the controlled catalytic pathway compared to the M-N-C fraction, weakening the adsorption of oxygen intermediates and shifting the ORR from the $4e^-$ to $2e^-$ pathway [75]. For example, the ORR pathway on atomically dispersed Zn sites can be flexibly changed by tailoring the coordination environment of the catalytic center. Structures with unique C-O coordination (ZnO_3C) or C-N coordination (ZnN_4) can be prepared by changing the functional groups of the corresponding precursors. In contrast to ZnN_4, which produced H_2O via the $4e^-$ pathway, a controlled change in the coordination environment of the Zn site allowed ZnO_3C to produce H_2O_2 in 0.1 M KOH with a near-zero over-potential and high selectivity in the $2e^-$ pathway. It was shown by DFT calculations that the decrease in the electron density around Zn in ZnO_3C led to a downward shift of the *d*-band center of Zn away from the Fermi level, thus altering the adsorption strength of the *OOH intermediate and improving the reaction selectivity [86].

Introducing other nonmetal coordination atoms is also an efficient and general strategy to achieve applicable selectivity. Sulfur was employed to fabricate atom-dispersed metal-site catalysts to boost $2e^-$ ORR [10]. In some cases, when the O coordination in M-O_4 was changed to oxidized- or thiophene- S coordination, the carbon substrate would be endowed with electron-withdrawal or electron-donation property, respectively [87,88]. It is worth noting that the oxidized S part has electron-withdrawing property, which can reduce the *d*-band center position of the metal and the adsorption energy of the ORR intermediate. On the contrary, the thiophene S component with an electron-donating effect can enhance the adsorption ability of M-N_4 sites, thereby decreasing the $2e^-$ ORR performance. Fig. 6a-b depict the two primary atomic configurations. In addition, control experiments and DFT calculations showed that both the O/S content and the adjacent coordinated environment strongly affect H_2O_2 production activity [88]. Also, at the reaction equilibrium potential of H_2O_2 formation, the Mo central site of the Mo-O_4-C portion exhibited a positive intermediate free energy, as shown in Fig. 6c. However, the introduction of S can significantly reduce the energy barrier of $2e^-$ ORR by affecting the intermediate *OOH adsorption behavior. Another doping method is to dope heteroatoms near the active site without changing the M-N_4 species [89–91]. Yan et al [90] found that the charge of Sb atom tends to stabilize after doping S near SbN_4, and the coordination N and outer-sphere S atoms can modulate the charge state of Sb thus affecting its interaction with *OOH intermediates. Theoretical calculations also revealed that porphyrinic-SbN_4-S has the most suitable *OOH binding energy and the highest thermodynamic limiting potential, indicating that the $2e^-$ pathway is more energetically favorable. The above clues clearly revealed the importance of local coordination structures in optimizing the electronic structure of atomically dispersed metal catalysts and intermediate adsorption strength, so that the catalytic performance has good adjustability.

B and P with quasi-metallic properties and relatively weak electronegativity are other viable coordination elements, and they can effectively modulate the electronic structure of the central active metal [92–94]. For example, the doping of B can change the electronic structure of Ni, and the strong interaction between the 2*p* electrons of B and the 2*s* electrons of O_2 facilitated the maintenance of the O-O bond [92]. After structural optimization, the most stably presented Ni_4-B_1 @BNC was shown to be more active and selective for the reduction of oxygen to H_2O_2. As shown in Fig. 6d, the doping of B changed the density of states of Ni-3*d* orbitals near the Fermi energy level, bringing the *d*-band center of Ni_4-B_1 @BNC closer to the Fermi level and enhancing the adsorption of O_2 and intermediates. Liu et al [94] doped P atoms into carbon substrates and synthesized the P-doped Co SACs catalysts. Various bonding configurations of P dopants in N-doped carbon substrate were first investigated and the binding energy in each configuration was calculated. The introduction of P atoms led to an extension of the Co-N bond length and this extension degree highly depended on the amount of doped P atom (Fig. 6e). P-doping modulated the electronic structure of the Co site, which endowed P_2-Co-N_4 a weaker *OOH binding energy and a higher thermodynamic limiting potential (Fig. 6f).

In addition to adding other heteroatoms for coordination, the same effect can be achieved by directly adding the same N atoms for coordination, and the different composition types of the coordinated N affect the selectivity of the catalyst. Ye et al [95] constructed Zn-MOF-74 derived N-doped mesoporous carbon catalysts and systematically investigated the different types and amounts of N composition induced by using different calcination temperatures. By increasing the temperature to 1000 ℃, the Zn-N interaction gradually decreased and faded out, and the relative content of graphite-N gradually increased, while pyrrole-N decreased. The total ratio of pyridine-N to graphite-N reached the highest value of 70.23% at 1000 ℃ and the catalyst exhibited the highest ORR performance at 800 ℃ or 900 ℃ compared to other

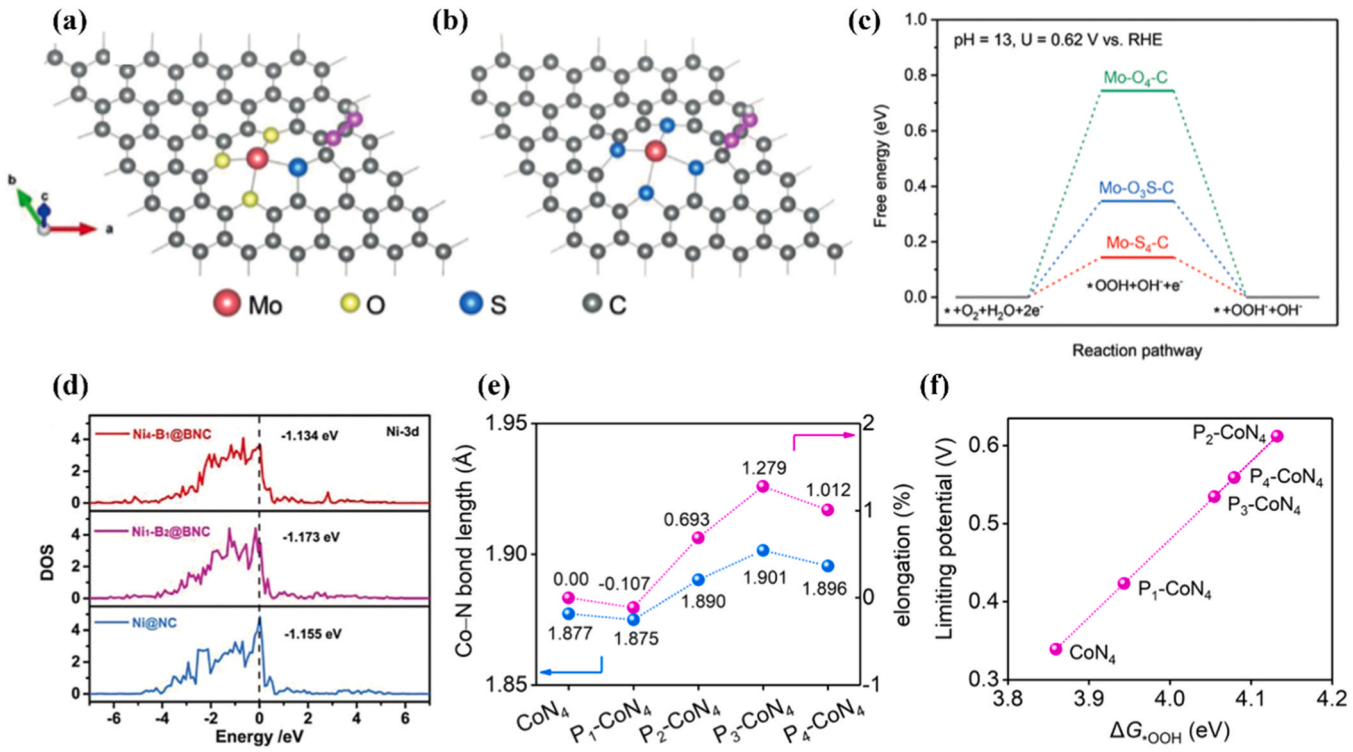

Fig. 6. (a) Atomic configuration of *OOH adsorption on Mo-O_3S-C. (b) Atomic configuration of *OOH adsorption on Mo-S_4-C. (c) Free energy diagram of 2e$^-$ ORR on three investigated substrates at equilibrium potential of the reaction. (d) Densities of states for Ni-3*d*. (e) Influence of doped P amount on the mean bond length and elongation of Co-N bond in the CoN_4 moiety. (f) Limiting potentials as a function of ΔG_{*OOH} for different contents of P dopants.
(a-c) Adapted with permission from [88]. Copyright 2020 Wiley OnlineLibrary. (d) Adapted with permission from [93]. Copyright 2022 Wiley OnlineLibrary. (e-f) Adapted with permission from [94]. Copyright 2022 Elsevier.

catalysts (Fig. 7a-b). Thus, the content of pyridine-N and graphite-N was correlated with the activity of 4e$^-$ ORR, while pyrrole-N was correlated with the selectivity of 2e$^-$ ORR.

Besides the doping atom types, changing the coordination atom number of the catalyst can also be employed to optimize the catalyst performance. Typically, the metal center of M-N_x-C catalysts is coordinated to four nitrogen atoms, which are thermodynamically stable. However, this coordination structure does not always have the optimal binding energy toward oxidation intermediates and thereby achieving the best catalytic performance [96,97]. The coordination number can then be tuned to change the electronic configuration of the metal center. Pyrolysis temperature is one of the widely adopted means to tune coordination number. Fan et al [98] regulated the coordination number of N in Pt-N_x-C by varying the carbonization temperature, and the N content gradually decreased as the calcination temperature increased. At low calcination temperatures (800 and 900 ℃), the abundant N content ensured high Pt-N coordination and the formation of a stable atomic dispersion structure. High temperature destroyed the Pt-N coordination environment and led to a partial aggregation of Pt atoms as nanoparticles (Fig. 7c-d). The modulating effect of variable coordinated N atoms on catalytic activity can be further demonstrated by DFT calculations. As the coordinated N atoms number decreased, the free energy of Pt-N_x-C gradually decreased, and Pt-N_1-C showed the lowest free energy and exhibited a lower energy potential. Based on the catalytic reaction energy barrier in Pt-N_1-C [98], they proposed an oxygen reduction reaction pathway (Fig. 7e) and confirmed that the O_2 molecule was adsorbed on Pt atom with double bond to form *OOH intermediate. The O_2 adsorption with double bond mechanism makes the O-O bond break more easily than that the adsorption mechanism of two O atoms on Pt atoms. The increase of the number of N coordination sites was also beneficial for Pt atom's association with the *OOH intermediate and the improvement of 2e$^-$ ORR selectivity.

For certain catalytic sites with a strong adsorption to O intermediate, lowering the coordination number can enhance the adsorption energy of the intermediate and thus reduce the 4e$^-$ ORR selectivity. A recent study of W SACs verified this point [99]. In this work, W_1/NO-C contained an anomalous tridentate $W_1N_1O_2$ coordination structure in which a W atom is coordinated to two O atoms and one N atom, was synthesized and exhibited an extraordinary performance of H_2O_2 electrosynthesis. Theoretical calculations determined that the O-adjacent C atom in the $W_1N_1O_2$-C part is the active site for the 2e$^-$ ORR and OH^- adsorption at the central W atom played a crucial role in optimizing the binding energy of the *OOH intermediate. Hydroxyl groups can be spontaneously attached to the W metal center in alkaline media, which facilitated the transformation of the oxygen reduction reaction from the 4e$^-$ to the 2e$^-$ pathway (Fig. 7f). The reduction in the number of N coordination sites will avoid the binding of the *O intermediate to the metal atom, decreasing the 4e$^-$ ORR selectivity.

4.2. *Activity improvement via substrate optimization*

Recent experimental and theoretical investigations have clearly shown that isolated metal atoms can be tightly bound to the substrate through covalent and electronic interactions [100,101]. Moreover, the electronic structure of isolated metal atoms can be greatly influenced by substrates, thus selecting an appropriate substrate may boost the catalytic activity [56,102,103]. Carbon compounds are viewed as promising catalysts for 2e$^-$ ORR, by considering their merits of high adjustability and environmental benign [16]. Although heteroatom doping and material structure tuning can improve its activity, high over-potential greatly restricts the geometric current density during H_2O_2 generation [15,23]. Nevertheless, carbon-based materials are outstanding carriers for anchoring single metal atoms due to their high specific surface area and superb electrical conductivity. Currently, various dimensions of

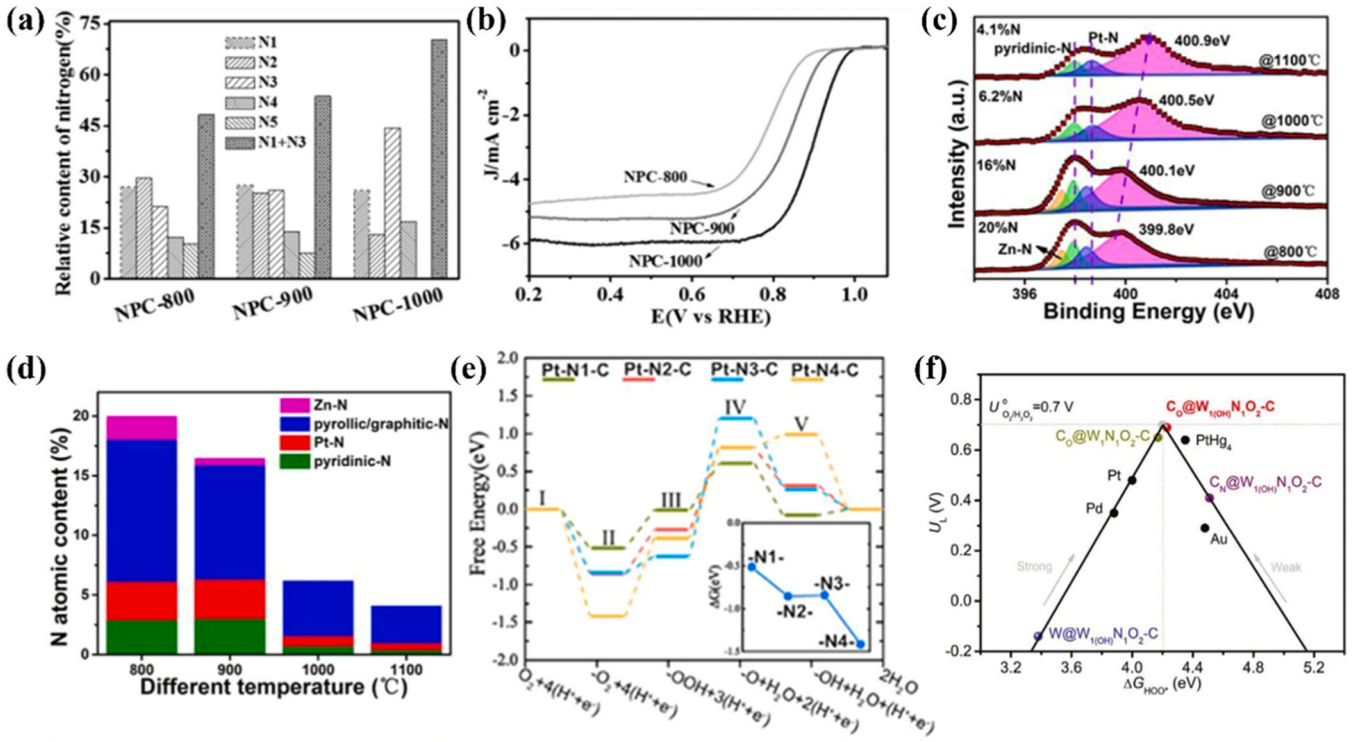

Fig. 7. (a) The variation of the four kinds of nitrogen species after calcinating at different temperatures. (b) Linear sweep voltammetry curves of NPC calcinating at different temperatures. (c) The high-resolution N 1s of Pt-NC-1.5% samples prepared under different calcination temperatures of 800-1100 ℃. (d) The contents of N configurations in the Pt-NC-1.5% samples at various temperatures. (e) The free energy diagrams on different Pt-N_x-C catalysts. (f) The calculated ORR activity volcano plot for $2e^-$ pathway to H_2O_2.
(a-b) Adapted with permission from [95]. Copyright 2017 Wiley OnlineLibrary. (c-e) Adapted with permission from [98]. Copyright 2021 Elsevier. (f)Adapted with permission from [99]. Copyright 2022 Wiley Online Library.

carbon materials including carbon black [104], carbon nanosphere [105], graphene [106], carbon nanorod [107], etc., have been used as SACs carriers. Due to their distinct structural features and physicochemical properties, these carbon materials have demonstrated their advantages in improving SACs activity [108–110]. For example, the abundant intrinsic defects on the 2D nanosheet surface can provide sites to fix and mass load metal atom. Additionally, adding a single metal atom to a metal-free 2D nanosheet like graphene, g-C_3N_4 or graphene diyne can significantly alter the electrical structure of nearby carbon atoms, creating extra active sites for various catalytic processes [106]. Daniel et al [106] synthesized a new graphene-based hybrid nanomaterial: nanowire-templated three-dimensional fuzzy graphene (NT-3DFG), and precisely controlled the size and density of the out-of-plane graphene flakes and edges through an adjustable synthesis procedure (Figs. 8a and b). The NT-3DFG electrode showed an adjustable ORR active site density, thereby performing an excellent H_2O_2 production, with onset potential of 0.79 ± 0.01 V *vs.* RHE and selectivity of 94 ± 2%.

The shape of the carbon substrate greatly affects its electrical configuration [111]. Due to the difference in the configurations of the carbon substrate, Fe-N_4 material can exist in various forms of Fe-N_{2+2}, FeN_4-C_8, FeN_4-C_{10} and FeN_4-C_{12}. The Fe-N_{2+2} is not active for ORR reaction, because the fully filled d_z^2 orbital hinders the formation of σ-bond with O_2, which makes the subsequent reduction reaction almost impossible to proceed. Liu et al [112] found that different carbon structures affect the binding energy of the *OOH intermediate and the catalyst activity (Fig. 8c). Heteroatoms doping is the widely adopted strategy to improve the SACs activity, and this will also change the substrate characteristics. Additional lone pairs of electrons exist when metals are doped into the carbon lattice network. Nitrogen is the most popular heteroatom that accelerates electron transfer via optimizing the electronic properties of carbon carriers. Normally, high N content provides abundant active sites, such as pyridine N and pyrrole N, which can theoretically increase the reaction rate. However, when the N content is too high, it may also lead to a reduced conductivity and expose more sites susceptible to poisoning [113]. It is worth noting that different parameters, such as the geometry of the carrier, N-species formation, crystallinity, valence state of the central metal atom, etc., will all affect the electrochemical performance, and it is difficult to intentionally change a parameter to a large extent without affecting other parameters [114]. FeN_4 on different carbon supports has different electronic structures, so that it appears different O_2 adsorption configurations and undergoes different structural transformations.

In addition to planar active carbon substrates, CNT provides ideal model substrates for studying the structure-function relationships of SACs due to their well-defined and homogeneous sp^2 hybridized carbon networks [115,116]. Compared with two-dimensional structures, CNT have more sp^2-like C atoms and strained C-C bonds due to geometric bending [117]. The bent carbon substrate may lead to a unique dynamic evolution of the active site, which precisely controls the catalytic process. Han et al [118] demonstrated that substrates of CuN_2C_2 SACs embedded within the sp^2-hybridized carbon framework showed an enhanced activity. While at the same time they introduced oxygen functional groups to modulate the adsorption strength of O_2 molecules and achieved the improved ORR activity by up to six folds. A charge density difference analysis was performed to assess the electron transfer property between the active site and the intermediate (Fig. 8d). It was found that more negative charges were transferred to $*O_2$ on the less curved Cu/CNT-8, which led to a more favorable protonation of $*O_2$. Sufficient electron transfer further promoted the reduction of the adsorbed intermediates and thus ORR activity, which was in good agreement with the experimental results. In another similar study, Lee et al [91] found that the generation of electron-deficient phthalocyanine Co (CoPC) in the presence of oxygen functional groups on the CNT

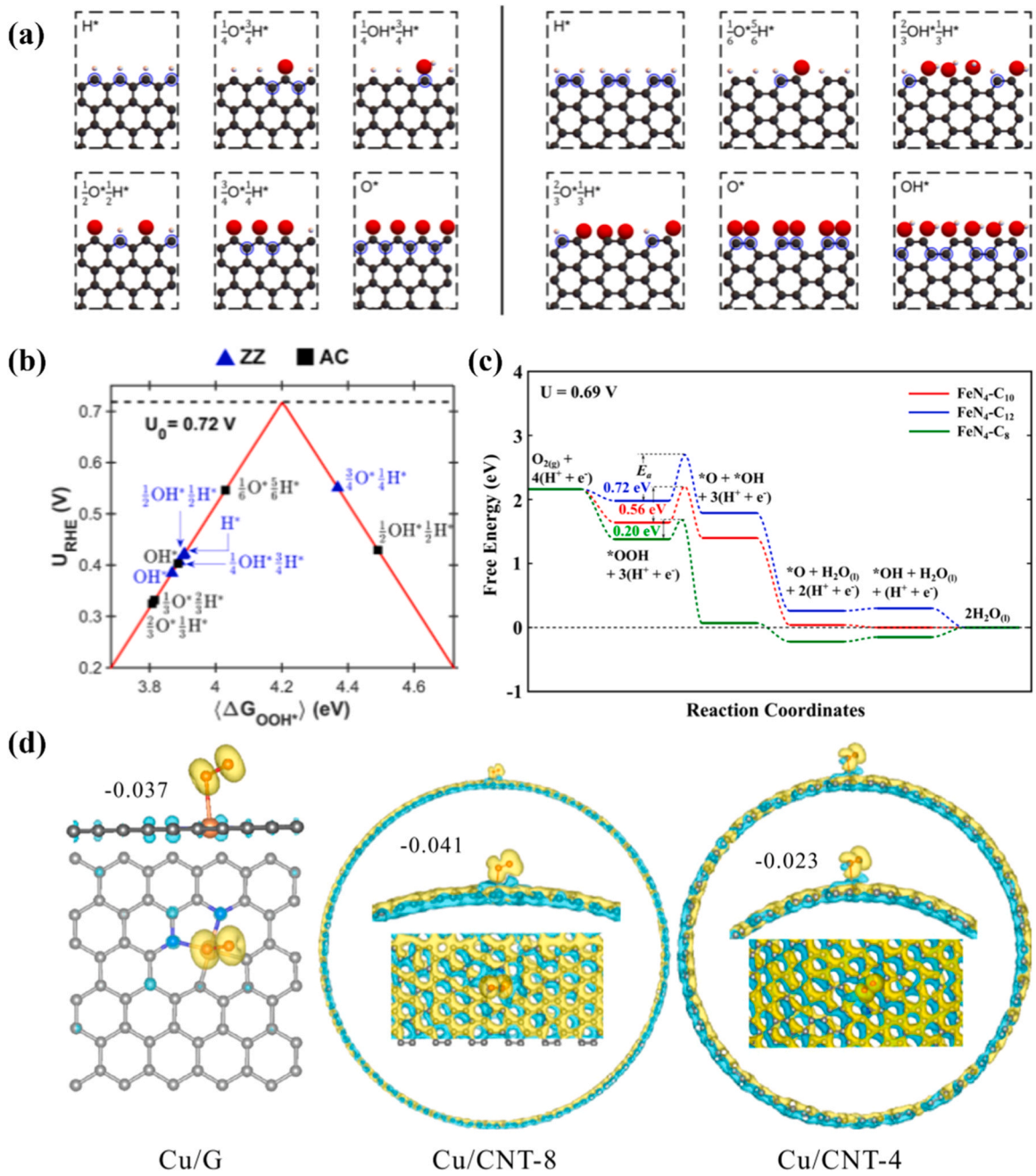

Fig. 8. (a) Representative set of termination configurations of zigzag (ZZ) and armchair (AC) edge configurations with circled atoms showing the determined most stable active site for hydrogen peroxide formation. (b) Theoretical activity volcano for 2e$^-$ ORR showing the activity predictions of various surface states. (c) Calculated free energy evolution diagrams for the O_2 reduction through an *OOH dissociation pathway on the active sites FeN_4-C_{10}, FeN_4-C_{12}, and FeN_4-C_8. (d) Side view and top view of the charge density difference for three models with $*O_2$, where yellow and blue areas represent higher and lower charge density, respectively. (a-b) Adaptedwith permission from [106]. Copyright 2020 American Chemical Society. (c)Adapted with permission from [112]. Copyright 2017 American Chemical Society.(d) Adapted with permission from [118]. Copyright 2021 Nature Publishing Group.

(OCNT) surface could modulate the interaction of the active site with the intermediate. The above catalyst exhibited an over-potential of 280 mV at 300 mA cm^{-2} electric density in neutral medium. Comparing OCNT with the pristine CNT substrate, epoxide group on CNT led to an electron leaving domain on the Co center, causing the *d*-band center of Co downward shifted. The epoxy group created an uneven charge distribution on the CNT surface, which induced dipole attraction between the carbon ring of CoPc and the CNT surface. The induced dipole led to a stronger π-π interaction and electron transfer performance between the CoPc and CNT surfaces, thereby improving the catalyst activity. It should be noted that the substrate change not only modulates the SACs activity, but also unavoidably affects the stability and selectivity of the catalysts.

4.3. O_2 adsorption configuration tunning via geometric effect

In addition to optimize the intermediate *OOH adsorption onto active sites, attention should also be paid to regulating adsorption configuration of O_2 molecule for a 2e$^-$ ORR SACs. Undispersed metal active centers often display two structural O_2 adsorption configurations, i.e., the Griffiths-type and the Yeager-type. The Griffiths-type configuration denotes the adsorption of O_2 on a single metal center whereas the

Yeager-type involves the adsorption of O_2 onto two neighboring metal centers [41,48,119]. The above two adsorption types do not favor the conversion of O_2 to H_2O_2, from the standpoint of adsorption energy. In contrast, the Pauling-type O_2 adsorption configuration is observed on SACs. The Pauling-type, which is categorized as a weaker adsorption and preferable for $2e^-$ ORR, is an end adsorption in which only one O atom adsorbs with a metal atom (Fig. 9a) [41]. The end O_2 adsorption has a higher preference among the three O_2 adsorption configurations for SACs. Since the metal active sites are distributed at atomic scale, there is a significantly lower chance of O-O bond breakage, indicating that SACs have an inherent advantage for H_2O_2 production via $2e^-$ ORR [40]. Rational design of SACs to avoid the side-on adsorption configuration of O_2 is then beneficial for H_2O_2 production.

The surface geometric design of the catalyst may change the O_2 adsorption configuration and then improve the $2e^-$ ORR selectivity. Many DFT theoretical investigations have demonstrated that the significant O_2 adsorption on the noble metal surface causes the breaking of the O-O bond [29,120–122]. For instance, O_2 prefers the Griffiths-type and Yeager-type adsorption types on the Pt/C surface before being reduced to H_2O through the $4e^-$ pathway (Fig. 9b) [123]. This, however, can be adjusted via geometric arrangement of atoms on the catalyst surface. When Pt is coated with carbon, O_2 is adsorbed end-to-end, which slowed down the breakup of the O-O bond and promoted the synthesis of H_2O_2 (Fig. 9c). The carbon layer also prevented H_2O_2 from being further dissociated on the Pt surface. Another common approach is to control the numbers of exposed active site. As the number of Pd atoms increases, the active site will shift from single atoms to atomic clusters, which affects the geometric structure of the active site. Calculations revealed that the C_4Pd_1 had a smaller *OOH adsorption energy, leading to better H_2O_2 production performance. However, there are also $*O_2$, *OO and *H adsorbates at the active site, which influence the selectivity of the catalyst. Therefore, it is equally important to investigate the adsorption energy for other intermediates. Wei et al [57] clarified that by controlling catalyst active sites at atomic-level distribution, O_2 adsorption would shift to the more thermodynamically advantageous end-on adsorption configuration while the presence of *OO and *H intermediates was greatly reduced.

Substrate structure was also crucial in determining the O_2 adsorption configuration. Several models involving FeN_4 fraction embedded in carbon have been proposed to explain the difference in ORR activity between Fe-N-C catalysts [112]. Fig. 9d shows the optimized atomic structure of O_2 adsorption configuration on FeN_4 sites that loaded on different carbon substrates. It was observed that despite the active sites were identical, different substrates resulted in disparate O_2 adsorption configurations. As predicted by DFT calculations, the binding strength of O_2 to the active site became stronger as the FeN_4 surrounded carbon atoms decreased, gradually forming the side-on adsorption configuration. Under side-on adsorption configuration Fe-O bonding orbitals were below the Fermi level, which were deeper than those of other two O_2 adsorption configurations. By analyzing the orientation of the Fermi level near the Fe-unbonded *d*-type orbitals, the binding strength and O_2 adsorption configuration can be predicted, which can provide theorical guidance for the design of SACs. In conclusion, in addition to the traditional selectivity enhancement based on tunning *OOH intermediates, the modification of SACs based on geometric effects can also lead to a good electrocatalytic performance [117,124].

5. Factors affecting the stability of SACs

For an industrial-scale production of H_2O_2 by SACs, catalyst stability is one of the most important issues that needs to be well addressed. Isolated metal atoms tend to aggregate to form metal clusters or nanoparticles during catalysis reaction, and the stability of SACs has become an enduring debate and to some extent an obstacle to their wide application [125,126]. First of all, the intrinsic structure of catalyst would directly affect its stability and should be considered at the beginning of

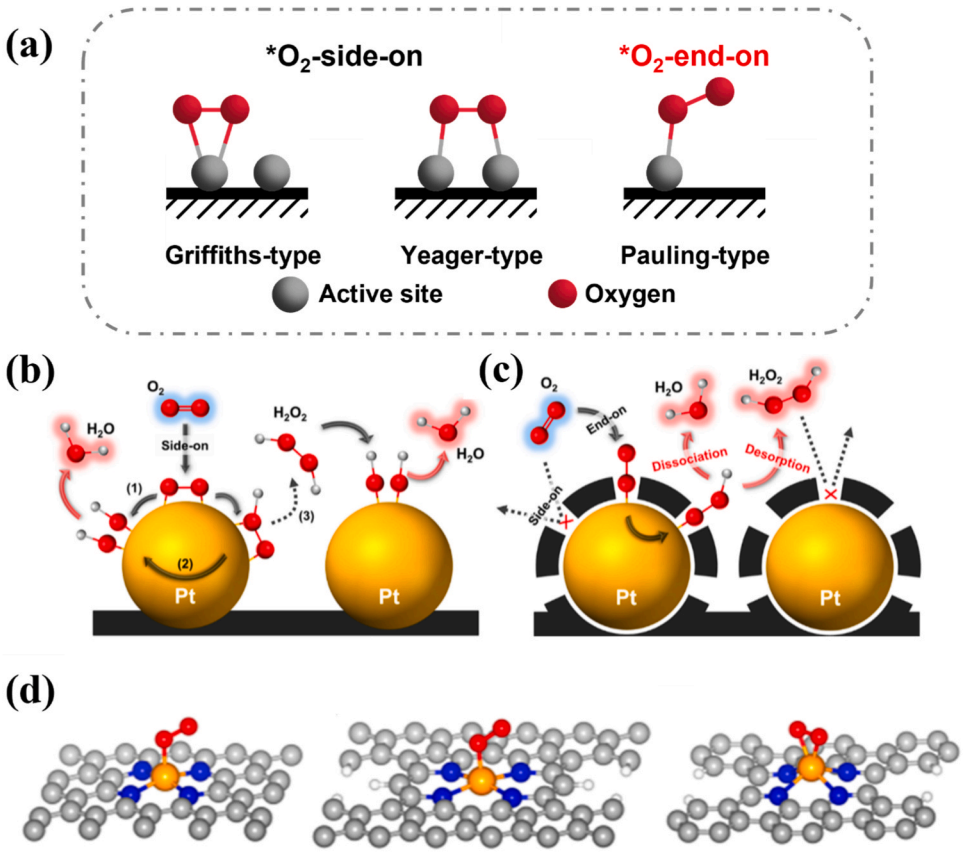

Fig. 9. (a) Schematic illustration of the different structures of O_2 adsorbed on active sites. (b) ORR pathways on the pristine Pt/C: O_2 prefers to adsorb on the Pt surface in a side-on configuration and then reduces to H_2O. (c) ORR pathways on the carbon-coated Pt: O_2 absorbs on the Pt surface in an end-on configuration and then produces H_2O and H_2O_2 as end products. (d) O_2 adsorption with an end-on configuration on FeN_4-C_{10}, FeN_4-C_{12}, and a side-on configuration on FeN_4-C_8.
(b-c) Adaptedwith permission from [123]. Copyright 2014 American Chemical Society. (d) Adapted with permission from [112]. Copyright 2017 American Chemical Society.

the catalyst design. For example, metal leaching or interfering ions will inevitably deteriorate the catalytic activity of the catalyst [127,128]. The substrate type, coordination environment and geometry of SACs not only modulate the activity and selectivity of the catalysts but also the stability, which has been well studied. However, most studies focused on short-term stability evaluation, tested by RRDE or H-cell device for no more than 24 h [125,129]. A longer duration of H_2O_2 production is essential to meet the industrial requirement [43]. Most of the current SACs with activated carbon substrates have shown the advantages of high activity and selectivity, but the carbon substrates are susceptible to corrosion at high oxidation potentials and oxygen concentration, resulting in declined catalyst stability [126,127]. Kumar et al [128] prepared Fe-N-C SACs and evaluated its stability under the NH_3 corrosion condition. Results showed that the graphitization degree of the carbon substrate was a key factor in determining the susceptibility of the SACs to corrosion, in addition to the active site of the catalyst.

Also, the accumulated H_2O_2 may present oxidative stress to SACs. It was found that when the materials were exposed to high concentrations of H_2O_2, the active sites or carbon substrates of the catalysts were subjected to aging due to the irreversible damage caused by H_2O_2 decomposition [130]. In addition to the common activated carbon based SACs, metal oxide or metal nitride substrates have been shown to be highly active and selective electrocatalysts [131]. However, the H_2O_2 corrosion and active site detachment would lead to a poor long-term stability of these metal oxides during catalyzing $2e^-$ ORR. The catalytic activity of Pt1/TiN was severely inhibited and surface passivation occurred after stability testing. X-ray photoelectron spectroscopy measurements confirmed that the TiN substrate was completely oxidized to TiO_2 (Fig. 10a), which resulted in the detachment of the original single Pt active site [56]. Non-carbon substrates normally affect the electron distribution of the metal active center and lead to a poor stability, which is one of the main reasons why activated carbon is now widely used as a substrate. However, this is not always the case for all non-carbon substrates. Villegas et al [132] analyzed the catalytic properties of a range of metals anchored on SnO_2 substrates. SnO_2 is a low-cost and corrosion-resistant substrate, and moreover, it remains stable over a wide range of pH and applied potentials. In addition to metal - substrate interactions, the electronegativity differences between the individual metals and nearby Sn atoms also affect the stability of SACs. Herein, a more stable single atom structure anchored on SnO_2 can be expected via optimizing the metal loading amount, to avoiding metal leaching or agglomeration.

Metal active sites shedding remains as another fundamental reason for the poor stability of SACs [133–135]. For SACs using carbon base as substrate, the corrosion of carbon substrates next to individual metal active sites may in turn aggravate the active metal sites leaching, creating a vicious cycle. Metal coordination environment not only induces the electronic effect but also determines the stability of the atomic structure. By modifying the coordination sites of the substrate, it may strengthen the interaction between metal atoms and substrate, further

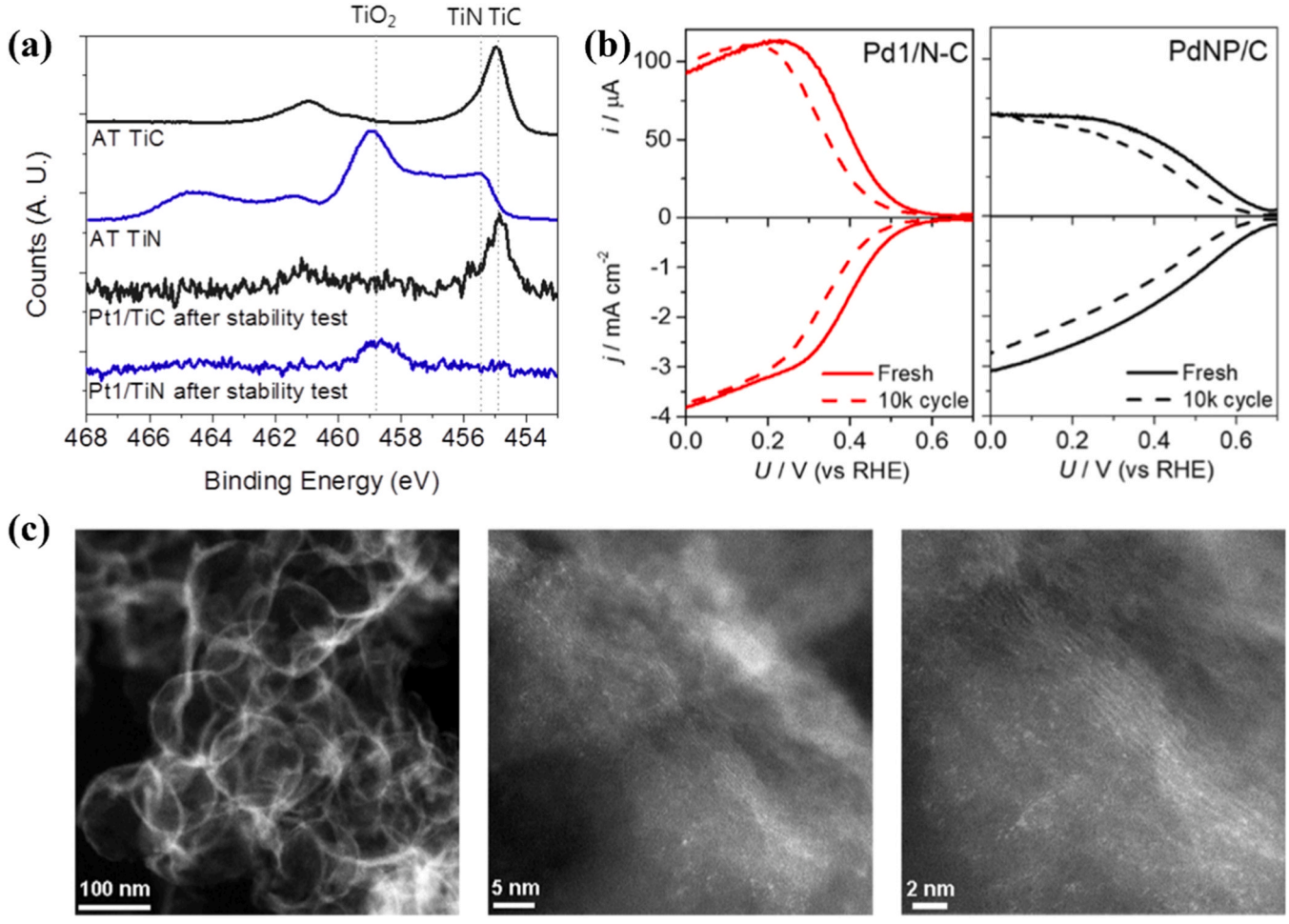

Fig. 10. (a) Ti 2p XPS spectra of TiC and TiN after acid treatment (AT) and 0.2 *wt.*% Pt1/TiC and 0.2 *wt.*% Pt1/TiN samples after 5000 cycle of cyclic voltammetry stability test. (b) ORR performance of Pd1/N-C and PdNP/C using a rotating ring-disk electrode before and after 10,000 cycles "on-off" durability test. (c) Aberration-corrected HAADF-STEM image of Pd1/N-C SAC and enlarged HAADF-STEM image after 10,000 cycles of "on-off" test.
(a) Adaptedwith permission from [56]. Copyright 2016 American Chemical Society. (b-c)Adapted with permission from [136]. Copyright 2021 Elsevier.

avoiding the leaching out of metal atoms under acidic conditions. Xi et al [136] proposed a strategy to overcome the stability problem by anchoring Pd atoms on modified hollow carbon nanospheres to enhance the ability of the active site. They evaluated the stability of the catalyst using "on-off" accelerated durability experiments. After 10,000 tests, the ring current of Pd1/N-C was slightly negatively shifted, and the peak current was almost unchanged (Fig. 10b). This indicates that while the 2e-pathway is deactivated to some extent, the 4e-pathway also undergoes a similar deactivation after testing, which resulted in a net unchanged selectivity. Pd1/N-C highlights the improved stability compared to the other samples (Fig. 10c). The doped N atoms can provide electron density to Pd^{2+} and enhance the binding strength to Pd species, thus leading to an improved stability.

Performance degradation may be also derived from the further reduction of the generated H_2O_2, especially when Fe-SACs are used. The possible non-homogeneous Fenton reaction of Fe with H_2O_2 brings not only catalyst corrosion issue but also greatly reduces the H_2O_2 yield. In particular, when Fe catalyzes the decomposition of H_2O_2 through the typical Fenton reaction, a high concentration of reactive oxygen species will be generated, which will directly lead to oxidation, corrosion and eventual metal shedding on the carbon surface [137,138]. Therefore, in addition to avoiding the use of Fe-containing catalysts and reducing Fe contamination, using core-shell structures or enhancing the interaction between Fe and substrate to avoid metal shedding are effective strategies. Overall, the current research on H_2O_2 production processes is limited and the stability issues of $2e^-$ ORR processes are still huge challenges at present.

6. Future perspective and Summary

Despite intensive studies have been conducted in recent years, the efficient production of H_2O_2 by $2e^-$ ORR and the exploration of suitable in situ applications of the generated H_2O_2 remain challenged. Several SACs still suffer from low catalytic efficiency, unclear catalytic sites, and poor stability. The ideal catalyst for H_2O_2 generation by $2e^-$ ORR implies that the adsorption of *OOH should be maintained at a moderate strength. The selectivity of the catalyst is related to its ability to break the O-O bond. The study of SACs that breaks the inherent intermediate ratio relationship will greatly advance the progress of $2e^-$ ORR for the H_2O_2 generation. For practical applications, $2e^-$ ORR catalysts should also have excellent activity, conductivity, and mass transfer properties. Furthermore, the application of H_2O_2 generation by $2e^-$ ORR electrochemistry can be intensively developed by various in situ devices, which is attractive in many scientific fields. In the further development of ideal $2e^-$ ORR SACs and promotion of its wide range of applications, future research may be required to focus on the following areas.

Firstly, a feasible and universal method for mass-production of SACs should be explored. Noble metal SACs have high catalytic efficiency, but the high price of catalysts and the scarcity of noble metals themselves increase its overall cost. In the future, we should develop efficient non-precious metals to achieve the comparable or even better catalyst performance to that of precious metals. Restricted by the preparation technology, the metal loading amount in SACs is generally low, which leads to the problem of the low active site content on the catalyst surface. Further increase in metal content is challenging because excessive addition of metal precursors may lead to agglomeration of metal species into clusters or nanoparticles during conventional pyrolytic synthesis. To address the above issue, several strategies including metal molecular grafting, spatially restricted domains, multilayer stabilization, and cascade anchoring were used to alleviate the agglomeration of metal atoms [131,139,140]. However, these strategies usually require complex steps. A simple and easy-to-operate SACs fabrication method aiming at high yields, metal loading, and mass production is still required in the future.

Secondary, SACs with an improved activity and stability for H_2O_2 production should be developed. Carbon-based carriers have high electrical conductivity and excellent mass transfer properties due to their special porous structure. More efforts should be focused on improving their catalytic efficiency through a theoretical study combining with experiment validation approach. The co-doping of SACs with transition metals and heteroatoms is an efficient strategy to improve their $2e^-$ ORR catalytic performance. However, there is no unified theoretical system to support when faced with complex co-doped structures, and the collaboration of multiple active sites on the catalyst surface leads to complex results. The research deciphering the mechanism of the co-interaction of transition metals, N-doping, and oxygen functional groups may be still required in the future work. Optimization of transition metal sites and functionalized carriers is essential to modulate the catalytic activity of SACs. Supporting by more advanced techniques such as high throughput screening studies, DFT calculations, and advanced characterization techniques, more efficient SACs might be developed. Besides the possibility of reducing the noble metal usage, bimetallic SACs have advantages of breaking the inherent adsorption ratio of intermediates, reducing over-potential, and improving catalyst stability. Exploring the appropriate double metal atoms type and adjusting their ratio might be effective to improve the H_2O_2 production via $2e^-$ ORR. More importantly, the issue of SACs stability must be addressed for its practical application. For SACs, stability remains a great challenge due to the possibility of aggregation or leaching during the catalytic process. Choosing a suitable carrier and improving the interaction between individual metal atoms and the carrier is one of the important strategies to solve stability problems. It is noteworthy that most of the current studies focused on the electrochemical generation of H_2O_2 in acidic and alkaline electrolytes, while studies in neutral electrolytes are limited. However, in practical situations, the application of H_2O_2 generated in acidic or alkaline media is often limited due to the influence of pH. Therefore, the generation of H_2O_2 in neutral aqueous solutions, which is also useful for environmental remediation, should be intensively studied.

Thirdly, the catalytic mechanism of $2e^-$ ORR on SACs should be more clearly clarified. Currently, SACs are largely underexploited due to the low density of metal atoms and the lack of understanding of structure-property correlations. Different factors, including carrier effects, heteroatom functional groups, transition metal species, ligand environment, solvation effects, and pH, are associated with catalytic sites activities and further affect the catalyst performance. However, the relationship between them was found to be unclear. Simultaneously, understanding which reaction steps are catalyzed by which sites are not profound. Therefore, intensive experimental and theoretical computational work is needed to elucidate the correlation between SACs catalytic sites and catalytic performance and then further reveal the general relationship between catalyst structure and the above factors. There has been a breakthrough in SACs targeting nitrogen atom doping, which is determined to be a combination of several functional groups. However, works conducted for oxygen functional groups is still lacking. How to directionally synthesize the necessary oxygen functional groups to assist SACs to achieve better selectivity is a worthy focus of the next research. In other words, there are limited studies on the targeted synthesis of SACs with different selectivity for different application purposes. However, to achieve the above objective, an in-depth understanding on the catalytic structure-performance relationship is of great significance.

In conclusion, $2e^-$ ORR is a promising green pathway to produce valuable H_2O_2. In order to overcome the current obstacles in this field, it is necessary to improve the activity, selectivity and stability of catalysts for catalytic reduction of O_2 to H_2O_2, as well as a wider field of view for practical scale-up and industrial requirements. Based on the latest research progress in the application of SACs in the field of $2e^-$ ORR, which is attempted to be described in this review, it is expected to achieve efficient, simple and clean industrial synthesis of H_2O_2 in the near future.

Declaration of Competing Interest

The authors declare that they have no known competing financial interests or personal relationships that could have appeared to influence the work reported in this paper.

Data Availability

The authors are unable or have chosen not to specify which data has been used.

Acknowledgments

This work was supported by the "Pioneer" and "Leading Goose" R&D Program of Zhejiang (2023C03149) and National Natural Science Foundation of China (51908172).

References

[1] J. Sun, Y. Wu, Anthraquinone redox relay for dye-sensitized photo-electrochemical H_2O_2 production, Angew. Chem. Int. Ed. 59 (2020) 10904–10908, https://doi.org/10.1002/anie.202003745.
[2] S. Yang, A. Verdaguer-Casadevall, L. Arnarson, L. Silvioli, V. Čolić, R. Frydendal, J. Rossmeisl, I. Chorkendorff, I.E.L. Stephens, Toward the decentralized electrochemical production of H_2O_2: a focus on the catalysis, ACS Catal. 8 (2018) 4064–4081, https://doi.org/10.1021/acscatal.8b00217.
[3] S. Fukuzumi, Y. Lee, W. Nam, Solar-driven production of hydrogen peroxide from water and dioxygen, Chem. – Eur. J. 24 (2018) 5016–5031, https://doi.org/10.1002/chem.201704512.
[4] C. Samanta, Direct synthesis of hydrogen peroxide from hydrogen and oxygen: an overview of recent developments in the process, Appl. Catal. Gen. 350 (2008) 133–149, https://doi.org/10.1016/j.apcata.2008.07.043.
[5] Y. Jiang, P. Ni, C. Chen, Y. Lu, P. Yang, B. Kong, A. Fisher, X. Wang, Selective electrochemical H_2O_2 production through two-electron oxygen electrochemistry, Adv. Energy Mater. 8 (2018) 1801909, https://doi.org/10.1002/aenm.201801909.
[6] K. Otsuka, I. Yamanaka, One step synthesis of hydrogen peroxide through fuel cell reaction, Electrochim. Acta 35 (1990) 319–322, https://doi.org/10.1016/0013-4686(90)87004-L.
[7] Y. Zeng, G. Wu, Electrocatalytic H_2O_2 generation for disinfection, Chin. J. Catal. 42 (2021) 2149–2163, https://doi.org/10.1016/S1872-2067(20)63781-0.
[8] M. Melchionna, P. Fornasiero, M. Prato, The rise of hydrogen peroxide as the main product by metal-free catalysis in oxygen reductions, Adv. Mater. 31 (2019) 1802920, https://doi.org/10.1002/adma.201802920.
[9] Y. Zhu, R. Zhu, Y. Xi, J. Zhu, G. Zhu, H. He, Strategies for enhancing the heterogeneous Fenton catalytic reactivity: a review, Appl. Catal. B Environ. 255 (2019), 117739, https://doi.org/10.1016/j.apcatb.2019.05.041.
[10] C.H. Choi, M. Kim, H.C. Kwon, S.J. Cho, S. Yun, H.-T. Kim, K.J.J. Mayrhofer, H. Kim, M. Choi, Tuning selectivity of electrochemical reactions by atomically dispersed platinum catalyst, Nat. Commun. 7 (2016) 10922, https://doi.org/10.1038/ncomms10922.
[11] A. Verdaguer-Casadevall, D. Deiana, M. Karamad, S. Siahrostami, P. Malacrida, T. W. Hansen, J. Rossmeisl, I. Chorkendorff, I.E.L. Stephens, Trends in the electrochemical synthesis of H_2O_2: enhancing activity and selectivity by electrocatalytic site engineering, Nano Lett. 14 (2014) 1603–1608, https://doi.org/10.1021/nl500037x.
[12] J. Zhang, J. Zhang, F. He, Y. Chen, J. Zhu, D. Wang, S. Mu, H.Y. Yang, Defect and doping Co-engineered non-metal nanocarbon ORR electrocatalyst, Nano-Micro Lett. 13 (2021) 65, https://doi.org/10.1007/s40820-020-00579-y.
[13] S. Siahrostami, A. Verdaguer-Casadevall, M. Karamad, Enabling direct H_2O_2 production through rational electrocatalyst design, Nat. Mater. 12 (2013) 1137–1143, https://doi.org/10.1038/NMAT3795.
[14] Z. Zheng, Y.H. Ng, D.-W. Wang, R. Amal, Epitaxial growth of Au-Pt-Ni nanorods for direct high selectivity H_2O_2 production, Adv. Mater. 28 (2016) 9949–9955, https://doi.org/10.1002/adma.201603662.
[15] D. Iglesias, A. Giuliani, M. Melchionna, S. Marchesan, A. Criado, L. Nasi, M. Bevilacqua, C. Tavagnacco, F. Vizza, M. Prato, P. Fornasiero, N-doped graphitized carbon nanohorns as a forefront electrocatalyst in highly selective O_2 reduction to H_2O_2, Chem 4 (2018) 106–123, https://doi.org/10.1016/j.chempr.2017.10.013.
[16] Z. Lu, G. Chen, S. Siahrostami, Z. Chen, K. Liu, J. Xie, L. Liao, T. Wu, D. Lin, Y. Liu, T.F. Jaramillo, J.K. Nørskov, Y. Cui, High-efficiency oxygen reduction to hydrogen peroxide catalysed by oxidized carbon materials, Nat. Catal. 1 (2018) 156–162, https://doi.org/10.1038/s41929-017-0017-x.
[17] I. Yamanaka, R. Ichihashi, T. Iwasaki, N. Nishimura, T. Murayama, W. Ueda, S. Takenaka, Electrocatalysis of heat-treated cobalt-porphyrin/carbon for hydrogen peroxide formation, Electrochim. Acta 108 (2013) 321–329, https://doi.org/10.1016/j.electacta.2013.06.072.
[18] Y. Pang, H. Xie, Y. Sun, M.-M. Titirici, G.-L. Chai, Electrochemical oxygen reduction for H_2O_2 production: catalysts, pH effects and mechanisms, J. Mater. Chem. A 8 (2020) 24996–25016, https://doi.org/10.1039/D0TA09122G.
[19] L. Li, C. Tang, Y. Zheng, B. Xia, X. Zhou, H. Xu, S. Qiao, Tailoring selectivity of electrochemical hydrogen peroxide generation by tunable pyrrolic-nitrogen-carbon, Adv. Energy Mater. 10 (2020) 2000789, https://doi.org/10.1002/aenm.202000789.
[20] C. Zhang, W. Liu, M. Song, J. Zhang, F. He, J. Wang, M. Xiong, J. Zhang, D. Wang, Pyranoid-O-dominated graphene-like nanocarbon for two-electron oxygen reduction reaction, Appl. Catal. B Environ. 307 (2022), 121173, https://doi.org/10.1016/j.apcatb.2022.121173.
[21] M. Liu, H. Su, W. Cheng, F. Yu, Y. Li, W. Zhou, H. Zhang, X. Sun, X. Zhang, S. Wei, Q. Liu, Synergetic dual-ion centers boosting metal organic framework alloy catalysts toward efficient two electron oxygen reduction, Small 18 (2022) 2202248, https://doi.org/10.1002/smll.202202248.
[22] Y.-C. Yin, Y. Shi, Y.-B. Sun, D.-R. Yang, Y. Liu, X.-H. Xia, Selective electrochemical generation of hydrogen peroxide from oxygen reduction on atomically dispersed platinum, ACS Appl. Energy Mater. 4 (2021) 10843–10848, https://doi.org/10.1021/acsaem.1c01817.
[23] Y. Sun, L. Silvioli, N.R. Sahraie, W. Ju, J. Li, A. Zitolo, S. Li, A. Bagger, L. Arnarson, X. Wang, T. Moeller, D. Bernsmeier, J. Rossmeisl, F. Jaouen, P. Strasser, Activity-selectivity trends in the electrochemical production of hydrogen peroxide over single-site metal-nitrogen-carbon catalysts, J. Am. Chem. Soc. 141 (2019) 12372–12381, https://doi.org/10.1021/jacs.9b05576.
[24] S. Ren, Q. Yu, X. Yu, P. Rong, L. Jiang, J. Jiang, Graphene-supported metal single-atom catalysts: a concise review, Sci. China Mater. 63 (2020) 903–920, https://doi.org/10.1007/s40843-019-1286-1.
[25] X. Liu, H. Liu, C. Chen, L. Zou, Y. Li, Q. Zhang, B. Yang, Z. Zou, H. Yang, Fe_2N nanoparticles boosting FeN_x moieties for highly efficient oxygen reduction reaction in Fe-N-C porous catalyst, Nano Res 12 (2019) 1651–1657, https://doi.org/10.1007/s12274-019-2415-7.
[26] L. Liu, A. Corma, Metal catalysts for heterogeneous catalysis: from single atoms to nanoclusters and nanoparticles, Chem. Rev. 118 (2018) 4981–5079, https://doi.org/10.1021/acs.chemrev.7b00776.
[27] Y. Jia, X. Xiong, D. Wang, X. Duan, K. Sun, Y. Li, L. Zheng, W. Lin, M. Dong, G. Zhang, W. Liu, X. Sun, Atomically dispersed Fe-N_4 modified with precisely located S for highly efficient oxygen reduction, Nano-Micro Lett. 12 (2020) 116, https://doi.org/10.1007/s40820-020-00456-8.
[28] R. Zhou, Y. Zheng, M. Jaroniec, S.-Z. Qiao, Determination of the electron transfer number for the oxygen reduction reaction: from theory to experiment, ACS Catal. 6 (2016) 4720–4728, https://doi.org/10.1021/acscatal.6b01581.
[29] Y. Jiao, Y. Zheng, M. Jaroniec, S.Z. Qiao, Design of electrocatalysts for oxygen- and hydrogen-involving energy conversion reactions, Chem. Soc. Rev. 44 (2015) 2060–2086, https://doi.org/10.1039/C4CS00470A.
[30] J. Gao, H. bin Yang, X. Huang, S.-F. Hung, W. Cai, C. Jia, S. Miao, H.M. Chen, X. Yang, Y. Huang, T. Zhang, B. Liu, Enabling direct H_2O_2 production in acidic media through rational design of transition metal single atom catalyst, Chem 6 (2020) 658–674, https://doi.org/10.1016/j.chempr.2019.12.008.
[31] V. Tripković, E. Skúlason, S. Siahrostami, J.K. Nørskov, J. Rossmeisl, The oxygen reduction reaction mechanism on Pt(111) from density functional theory calculations, Electrochim. Acta 55 (2010) 7975–7981, https://doi.org/10.1016/j.electacta.2010.02.056.
[32] Y. Nie, L. Li, Z. Wei, Recent advancements in Pt and Pt-free catalysts for oxygen reduction reaction, Chem. Soc. Rev. 44 (2015) 2168–2201, https://doi.org/10.1039/C4CS00484A.
[33] J. Liu, C.Q. Sun, W. Zhu, Origin of efficient oxygen reduction reaction on Pd monolayer supported on Pd-M (M=Ni, Fe) intermetallic alloy, Electrochim. Acta 282 (2018) 680–686, https://doi.org/10.1016/j.electacta.2018.06.041.
[34] J. Wang, Z. Huang, W. Liu, C. Chang, H. Tang, Z. Li, W. Chen, C. Jia, T. Yao, S. Wei, Y. Wu, Y. Li, Design of N-coordinated dual-metal sites: a stable and active Pt-free catalyst for acidic oxygen reduction reaction, J. Am. Chem. Soc. 139 (2017) 17281–17284, https://doi.org/10.1021/jacs.7b10385.
[35] J. Park, Y. Nabae, T. Hayakawa, M. Kakimoto, Highly selective two-electron oxygen reduction catalyzed by mesoporous nitrogen-doped carbon, ACS Catal. 4 (2014) 3749–3754, https://doi.org/10.1021/cs5008206.
[36] Y. Sun, I. Sinev, W. Ju, A. Bergmann, S. Dresp, S. Kühl, C. Spöri, H. Schmies, H. Wang, D. Bernsmeier, B. Paul, R. Schmack, R. Kraehnert, B. Roldan Cuenya, P. Strasser, Efficient electrochemical hydrogen peroxide production from molecular oxygen on nitrogen-doped mesoporous carbon catalysts, ACS Catal. 8 (2018) 2844–2856, https://doi.org/10.1021/acscatal.7b03464.
[37] Z. Cynthia G., Handbook of electrochemistry. Elsevier Science, 2007, https://doi.org/10.1016/B978-0-444-51958-0.X5000-9.
[38] A.C. Brezny, S.I. Johnson, S. Raugei, J.M. Mayer, Selectivity-determining steps in O_2 reduction catalyzed by iron (tetramesitylporphyrin), J. Am. Chem. Soc. 142 (2020) 4108–4113, https://doi.org/10.1021/jacs.9b13654.
[39] S. Siahrostami, S.J. Villegas, A.H. Bagherzadeh Mostaghimi, S. Back, A. B. Farimani, H. Wang, K.A. Persson, J. Montoya, A review on challenges and successes in atomic-scale design of catalysts for electrochemical synthesis of hydrogen peroxide, ACS Catal. 10 (2020) 7495–7511, https://doi.org/10.1021/acscatal.0c01641.
[40] M.L. Pegis, C.F. Wise, D.J. Martin, J.M. Mayer, Oxygen reduction by homogeneous molecular catalysts and electrocatalysts, Chem. Rev. 118 (2018) 2340–2391, https://doi.org/10.1021/acs.chemrev.7b00542.
[41] M.M. Montemore, M.A. van Spronsen, R.J. Madix, C.M. Friend, O_2 activation by metal surfaces: implications for bonding and reactivity on heterogeneous

catalysts, Chem. Rev. 118 (2018) 2816–2862, https://doi.org/10.1021/acs.chemrev.7b00217.
[42] X. Liao, R. Lu, L. Xia, Q. Liu, H. Wang, K. Zhao, Z. Wang, Y. Zhao, Density functional theory for electrocatalysis, ENERGY Environ. Mater. 5 (2022) 157–185, https://doi.org/10.1002/eem2.12204.
[43] P. Cao, X. Quan, X. Nie, K. Zhao, Y. Liu, S. Chen, H. Yu, J.G. Chen, Metal single-site catalyst design for electrocatalytic production of hydrogen peroxide at industrial-relevant currents, Nat. Commun. 14 (2023) 172, https://doi.org/10.1038/s41467-023-35839-z.
[44] E. Skúlason, V. Tripkovic, M.E. Björketun, S. Gudmundsdóttir, G. Karlberg, J. Rossmeisl, T. Bligaard, H. Jónsson, J.K. Nørskov, Modeling the electrochemical hydrogen oxidation and evolution reactions on the basis of density functional theory calculations, J. Phys. Chem. C. 114 (2010) 18182–18197, https://doi.org/10.1021/jp1048887.
[45] J.K. Nørskov, J. Rossmeisl, A. Logadottir, L. Lindqvist, J.R. Kitchin, T. Bligaard, H. Jónsson, Origin of the overpotential for oxygen reduction at a fuel-cell cathode, J. Phys. Chem. B 108 (2004) 17886–17892, https://doi.org/10.1021/jp047349j.
[46] S. Siahrostami, A. Verdaguer-Casdevall, M. Karamad, I. Chorkendorff, I.E. L. Stephens, J. Rossmeisl, Activity and selectivity for O_2 reduction to H_2O_2 on transition metal surfaces, ECS Trans. 58 (2013) 53–62, https://doi.org/10.1149/05802.0053ecst.
[47] K.S. Exner, Does a thermoneutral electrocatalyst correspond to the apex of a volcano plot for a simple two-electron process? Angew. Chem. Int. Ed. 59 (2020) 10236–10240, https://doi.org/10.1002/anie.202003688.
[48] J. Gao, B. Liu, Progress of electrochemical hydrogen peroxide synthesis over single atom catalysts, ACS Mater. Lett. 2 (2020) 1008–1024, https://doi.org/10.1021/acsmaterialslett.0c00189.
[49] A. Wang, J. Li, T. Zhang, Heterogeneous single-atom catalysis, Nat. Rev. Chem. 2 (2018) 65–81, https://doi.org/10.1038/s41570-018-0010-1.
[50] X. Song, N. Li, H. Zhang, H. Wang, L. Wang, Z. Bian, Promotion of hydrogen peroxide production on graphene-supported atomically dispersed platinum: effects of size on oxygen reduction reaction pathway, J. Power Sources 435 (2019), 226771, https://doi.org/10.1016/j.jpowsour.2019.226771.
[51] J.S. Jirkovský, I. Panas, E. Ahlberg, M. Halasa, S. Romani, D.J. Schiffrin, Single atom hot-spots at Au-Pd nanoalloys for electrocatalytic H_2O_2 production, J. Am. Chem. Soc. 133 (2011) 19432–19441, https://doi.org/10.1021/ja206477z.
[52] M. Dhiman, V. Polshettiwar, Supported single atom and pseudo-single atom of metals as sustainable heterogeneous nanocatalysts, ChemCatChem 10 (2018) 881–906, https://doi.org/10.1002/cctc.201701431.
[53] X. Song, N. Li, H. Zhang, L. Wang, Y. Yan, H. Wang, L. Wang, Z. Bian, Graphene-supported single nickel atom catalyst for highly selective and efficient hydrogen peroxide production, ACS Appl. Mater. Interfaces 12 (2020) 17519–17527, https://doi.org/10.1021/acsami.0c01278.
[54] W. Liu, C. Zhang, J. Zhang, X. Huang, M. Song, J. Li, F. He, H. Yang, J. Zhang, D. Wang, Tuning the atomic configuration of Co-N-C electrocatalyst enables highly-selective H_2O_2 production in acidic media, Appl. Catal. B Environ. 310 (2022), 121312, https://doi.org/10.1016/j.apcatb.2022.121312.
[55] J. Chen, Q. Ma, X. Zheng, Y. Fang, J. Wang, S. Dong, Kinetically restrained oxygen reduction to hydrogen peroxide with nearly 100% selectivity, Nat. Commun. 13 (2022) 2808, https://doi.org/10.1038/s41467-022-30411-7.
[56] S. Yang, Y.J. Tak, J. Kim, A. Soon, H. Lee, Support effects in single-atom platinum catalysts for electrochemical oxygen reduction, ACS Catal. 7 (2017) 1301–1307, https://doi.org/10.1021/acscatal.6b02899.
[57] Z. Wei, B. Deng, P. Chen, T. Zhao, S. Zhao, Palladium-based single atom catalysts for high-performance electrochemical production of hydrogen peroxide, Chem. Eng. J. 428 (2022), 131112, https://doi.org/10.1016/j.cej.2021.131112.
[58] M. Ledendecker, E. Pizzutilo, G. Malta, G.V. Fortunato, K.J.J. Mayrhofer, G. J. Hutchings, S.J. Freakley, Isolated Pd sites as selective catalysts for electrochemical and direct hydrogen peroxide synthesis, ACS Catal. 10 (2020) 5928–5938, https://doi.org/10.1021/acscatal.0c01305.
[59] R. Shen, W. Chen, Q. Peng, S. Lu, L. Zheng, X. Cao, Y. Wang, W. Zhu, J. Zhang, Z. Zhuang, C. Chen, D. Wang, Y. Li, High-concentration single atomic Pt sites on hollow CuS_x for selective O_2 reduction to H_2O_2 in acid solution, Chem 5 (2019) 2099–2110, https://doi.org/10.1016/j.chempr.2019.04.024.
[60] J. Zhao, C. Fu, K. Ye, Z. Liang, F. Jiang, S. Shen, X. Zhao, L. Ma, Z. Shadike, X. Wang, J. Zhang, K. Jiang, Manipulating the oxygen reduction reaction pathway on Pt-coordinated motifs, Nat. Commun. 13 (2022) 685, https://doi.org/10.1038/s41467-022-28346-0.
[61] Y. Kuwahara, R. Matsumura, H. Yamashita, Hollow titanosilicate nanospheres encapsulating PdAu alloy nanoparticles as reusable high-performance catalysts for a H_2O_2 -mediated one-pot oxidation reaction, J. Mater. Chem. A 7 (2019) 7221–7231, https://doi.org/10.1039/C9TA01481K.
[62] H.-E. Kim, I.H. Lee, J. Cho, S. Shin, H.C. Ham, J.Y. Kim, H. Lee, Palladium single-atom catalysts supported on $C@C_3N_4$ for electrochemical reactions, ChemElectroChem 6 (2019) 4757–4764, https://doi.org/10.1002/celc.201900772.
[63] S. Yu, X. Cheng, Y. Wang, B. Xiao, Y. Xing, J. Ren, Y. Lu, H. Li, C. Zhuang, G. Chen, High activity and selectivity of single palladium atom for oxygen hydrogenation to H_2O_2, Nat. Commun. 13 (2022) 4737, https://doi.org/10.1038/s41467-022-32450-6.
[64] J.H. Kim, D. Shin, J. Lee, D.S. Baek, T.J. Shin, Y.-T. Kim, H.Y. Jeong, J.H. Kwak, H. Kim, S.H. Joo, A general strategy to atomically dispersed precious metal catalysts for unravelling their catalytic trends for oxygen reduction reaction, ACS Nano 14 (2020) 1990–2001, https://doi.org/10.1021/acsnano.9b08494.
[65] J. Tang, S. Xu, K. Sun, X. Gao, A. Chen, S. Tian, D. Zhou, X. Sun, Recycling synthesis of single-atom Zn-nitrogen-carbon catalyst for electrocatalytic reduction of O_2 to H_2O_2, Sci. China Mater. (2022) 1–7, https://doi.org/10.1007/s40843-022-2054-5.
[66] Q. Ma, H. Jin, J. Zhu, Z. Li, H. Xu, B. Liu, Z. Zhang, J. Ma, S. Mu, Stabilizing Fe-N-C catalysts as model for oxygen reduction reaction, Adv. Sci. 8 (2021) 2102209, https://doi.org/10.1002/advs.202102209.
[67] S. Chen, T. Luo, X. Li, K. Chen, J. Fu, K. Liu, C. Cai, Q. Wang, H. Li, Y. Chen, C. Ma, L. Zhu, Y.-R. Lu, T.-S. Chan, M. Zhu, E. Cortés, M. Liu, Identification of the highly active Co-N_4 coordination motif for selective oxygen reduction to hydrogen peroxide, J. Am. Chem. Soc. 144 (2022) 14505–14516, https://doi.org/10.1021/jacs.2c01194.
[68] M. Jahan, Q. Bao, K.P. Loh, Electrocatalytically active graphene-porphyrin MOF composite for oxygen reduction reaction, J. Am. Chem. Soc. 134 (2012) 6707–6713, https://doi.org/10.1021/ja211433h.
[69] S. Siahrostami, M.E. Björketun, P. Strasser, J. Greeley, J. Rossmeisl, Tandem cathode for proton exchange membrane fuel cells, Phys. Chem. Chem. Phys. 15 (2013) 9326, https://doi.org/10.1039/c3cp51479j.
[70] J. Ding, J. Huang, Q. Zhang, Z. Wei, Q. He, Z. Chen, Y. Liu, X. Su, Y. Zhai, A hierarchical monolithic cobalt-single-atom electrode for efficient hydrogen peroxide production in acid, Catal. Sci. Technol. 12 (2022) 2416–2419, https://doi.org/10.1039/D2CY00427E.
[71] E. Jung, H. Shin, B.-H. Lee, V. Efremov, S. Lee, H.S. Lee, J. Kim, W. Hooch Antink, S. Park, K.-S. Lee, S.-P. Cho, J.S. Yoo, Y.-E. Sung, T. Hyeon, Atomic-level tuning of Co-N-C catalyst for high-performance electrochemical H_2O_2 production, Nat. Mater. 19 (2020) 436–442, https://doi.org/10.1038/s41563-019-0571-5.
[72] J. Shen, Y. Wen, H. Jiang, S. Yu, C. Dong, Y. Fan, B. Liu, C. Li, Identifying activity trends for the electrochemical production of H_2O_2 on M-N-C single-atom catalysts using theoretical kinetic computations, J. Phys. Chem. C. 126 (2022) 10388–10398, https://doi.org/10.1021/acs.jpcc.2c02803.
[73] H. Shen, N. Qiu, L. Yang, X. Guo, K. Zhang, T. Thomas, S. Du, Q. Zheng, J. P. Attfield, Y. Zhu, M. Yang, Boosting oxygen reduction for high-efficiency H_2O_2 electrosynthesis on oxygen-coordinated Co-N-C Catalysts, Small 18 (2022) 2200730, https://doi.org/10.1002/smll.202200730.
[74] Y. Tian, M. Li, Z. Wu, Q. Sun, D. Yuan, B. Johannessen, L. Xu, Y. Wang, Y. Dou, H. Zhao, S. Zhang, Edge-hosted atomic Co-N_4 sites on hierarchical porous carbon for highly selective two-electron oxygen reduction reaction, Angew. Chem. Int. Ed. 61 (2022), https://doi.org/10.1002/anie.202213296.
[75] K. Jiang, S. Back, A.J. Akey, C. Xia, Y. Hu, W. Liang, D. Schaak, E. Stavitski, J. K. Nørskov, S. Siahrostami, H. Wang, Highly selective oxygen reduction to hydrogen peroxide on transition metal single atom coordination, Nat. Commun. 10 (2019) 3997, https://doi.org/10.1038/s41467-019-11992-2.
[76] Y. Wang, R. Shi, L. Shang, G.I.N. Waterhouse, J. Zhao, Q. Zhang, L. Gu, T. Zhang, High-efficiency oxygen reduction to hydrogen peroxide catalyzed by nickel single-atom catalysts with tetradentate N_2O_2 coordination in a three-phase flow cell, Angew. Chem. Int. Ed. 59 (2020) 13057–13062, https://doi.org/10.1002/anie.202004841.
[77] G. Wei, X. Liu, Z. Zhao, C. Men, Y. Ding, S. Gao, Constructing ultrahigh-loading unsymmetrically coordinated Zn-N_3O single-atom sites with efficient oxygen reduction for H_2O_2 production, Chem. Eng. J. 455 (2023), 140721, https://doi.org/10.1016/j.cej.2022.140721.
[78] X. Long, J. Li, S. Xiao, K. Yan, Z. Wang, H. Chen, S. Yang, A strongly coupled graphene and FeNi double hydroxide hybrid as an excellent electrocatalyst for the oxygen evolution reaction, Angew. Chem. Int. Ed. 53 (2014) 7584–7588, https://doi.org/10.1002/anie.201402822.
[79] X. Li, W. Zhong, P. Cui, J. Li, J. Jiang, Design of efficient catalysts with double transition metal atoms on C_2N layer, J. Phys. Chem. Lett. 7 (2016) 1750–1755, https://doi.org/10.1021/acs.jpclett.6b00096.
[80] Y. Cao, J. Zhao, X. Zhong, G. Zhuang, S. Deng, Z. Wei, Z. Yao, J. Wang, Building highly active hybrid double-atom sites in C_2N for enhanced electrocatalytic hydrogen peroxide synthesis, Green, Energy Environ. 6 (2021) 846–857, https://doi.org/10.1016/j.gee.2020.12.006.
[81] L. Zhang, J.M.T.A. Fischer, Y. Jia, X. Yan, W. Xu, X. Wang, J. Chen, D. Yang, H. Liu, L. Zhuang, M. Hankel, D.J. Searles, K. Huang, S. Feng, C.L. Brown, X. Yao, Coordination of atomic Co-Pt coupling species at carbon defects as active sites for oxygen reduction reaction, J. Am. Chem. Soc. 140 (2018) 10757–10763, https://doi.org/10.1021/jacs.8b04647.
[82] V.A. Setyowati, M.F. Rois, W. Widiyastuti, S. Nurkhamidah, N. Saidatin, M. F. Febrianto, Comparative study of single and bimetal-nitrogen-doped carbon prepared by polymerization and direct pyrolysis, Results Eng. 13 (2022), 100332, https://doi.org/10.1016/j.rineng.2022.100332.
[83] Q. Liu, S. Cao, Y. Qiu, L. Zhao, Bimetallic Fe-Co promoting one-step growth of hierarchical nitrogen-doped carbon nanotubes/nanofibers for highly efficient oxygen reduction reaction, Mater. Sci. Eng. B 223 (2017) 159–166, https://doi.org/10.1016/j.mseb.2017.06.012.
[84] J. Wang, W. Liu, G. Luo, Z. Li, C. Zhao, H. Zhang, M. Zhu, Q. Xu, X. Wang, C. Zhao, Y. Qu, Z. Yang, T. Yao, Y. Li, Y. Lin, Y. Wu, Y. Li, Synergistic effect of well-defined dual sites boosting the oxygen reduction reaction, Energy Environ. Sci. 11 (2018) 3375–3379, https://doi.org/10.1039/C8EE02656D.
[85] W. Ye, S. Chen, Y. Lin, L. Yang, S. Chen, X. Zheng, Z. Qi, C. Wang, R. Long, M. Chen, J. Zhu, P. Gao, L. Song, J. Jiang, Y. Xiong, Precisely tuning the number of Fe atoms in clusters on N-doped carbon toward acidic oxygen reduction reaction, Chem 5 (2019) 2865–2878, https://doi.org/10.1016/j.chempr.2019.07.020.
[86] Y. Jia, Z. Xue, J. Yang, Q. Liu, J. Xian, Y. Zhong, Y. Sun, X. Zhang, Q. Liu, D. Yao, G. Li, Tailoring the electronic structure of an atomically dispersed zinc

electrocatalyst: coordination environment regulation for high selectivity oxygen reduction, Angew. Chem. Int. Ed. 61 (2022), https://doi.org/10.1002/anie.202110838.
[87] E. Zhang, L. Tao, J. An, J. Zhang, L. Meng, X. Zheng, Y. Wang, N. Li, S. Du, J. Zhang, D. Wang, Y. Li, Engineering the local atomic environments of indium single-atom catalysts for efficient electrochemical production of hydrogen peroxide, Angew. Chem. Int. Ed. 61 (2022), e202117347, https://doi.org/10.1002/anie.202117347.
[88] C. Tang, Y. Jiao, B. Shi, J. Liu, Z. Xie, X. Chen, Q. Zhang, S. Qiao, Coordination tunes selectivity: two-electron oxygen reduction on high-loading molybdenum single-atom catalysts, Angew. Chem. Int. Ed. 59 (2020) 9171–9176, https://doi.org/10.1002/anie.202003842.
[89] J. Qin, H. Liu, P. Zou, R. Zhang, C. Wang, H.L. Xin, Altering ligand fields in single-atom sites through second-shell anion modulation boosts the oxygen reduction reaction, J. Am. Chem. Soc. 144 (2022) 2197–2207, https://doi.org/10.1021/jacs.1c11331.
[90] M. Yan, Z. Wei, Z. Gong, B. Johannessen, G. Ye, G. He, J. Liu, S. Zhao, C. Cui, H. Fei, Sb_2S_3-templated synthesis of sulfur-doped Sb-N-C with hierarchical architecture and high metal loading for H_2O_2 electrosynthesis, Nat. Commun. 14 (2023) 368, https://doi.org/10.1038/s41467-023-36078-y.
[91] B.-H. Lee, H. Shin, A.S. Rasouli, H. Choubisa, P. Ou, R. Dorakhan, I. Grigioni, G. Lee, E. Shirzadi, R.K. Miao, J. Wicks, S. Park, H.S. Lee, J. Zhang, Y. Chen, Z. Chen, D. Sinton, T. Hyeon, Y.-E. Sung, E.H. Sargent, Supramolecular tuning of supported metal phthalocyanine catalysts for hydrogen peroxide electrosynthesis, Nat. Catal. 6 (2023) 234–243, https://doi.org/10.1038/s41929-023-00924-5.
[92] H. Fu, N. Zhang, F. Lai, L. Zhang, Z. Wu, H. Li, H. Zhu, T. Liu, Lattice strained B-doped Ni nanoparticles for efficient electrochemical H_2O_2 synthesis, Small 18 (2022) 2203510, https://doi.org/10.1002/smll.202203510.
[93] J. Pan, Q. Fang, Q. Xia, A. Hu, F. Sun, W. Zhang, Y. Yu, G. Zhuang, J. Jiang, J. Wang, Dual effect of the coordination field and sulphuric acid on the properties of a single-atom catalyst in the electrosynthesis of H_2O_2, Phys. Chem. Chem. Phys. 23 (2021) 21338–21349, https://doi.org/10.1039/D1CP03189A.
[94] J. Liu, Z. Wei, Z. Gong, M. Yan, Y. Hu, S. Zhao, G. Ye, H. Fei, Single-atom CoN_4 sites with elongated bonding induced by phosphorus doping for efficient H_2O_2 electrosynthesis, Appl. Catal. B Environ. 324 (2023), 122267, https://doi.org/10.1016/j.apcatb.2022.122267.
[95] L. Ye, G. Chai, Z. Wen, Zn-MOF-74 derived N-doped mesoporous carbon as pH-Universal electrocatalyst for oxygen reduction reaction, Adv. Funct. Mater. 27 (2017) 1606190, https://doi.org/10.1002/adfm.201606190.
[96] H. Gong, Z. Wei, Z. Gong, J. Liu, G. Ye, M. Yan, J. Dong, C. Allen, J. Liu, K. Huang, R. Liu, G. He, S. Zhao, H. Fei, Low-coordinated Co-N-C on oxygenated graphene for efficient electrocatalytic H_2O_2 production, Adv. Funct. Mater. 32 (2022) 2106886, https://doi.org/10.1002/adfm.202106886.
[97] C. Xiao, L. Cheng, Y. Zhu, G. Wang, L. Chen, Y. Wang, R. Chen, Y. Li, C. Li, Super-coordinated nickel N4Ni1O2 site single-atom catalyst for selective H2O2 electrosynthesis at high current densities, Angew. Chem. Int. Ed. n/a (n.d.) e202206544. https://doi.org/10.1002/anie.202206544.
[98] M. Fan, J. Cui, J. Zhang, J. Wu, S. Chen, L. Song, Z. Wang, A. Wang, R. Vajtai, Y. Wu, P.M. Ajayan, J. Jiang, D. Sun, The modulating effect of N coordination on single-atom catalysts researched by Pt-N_x-C model through both experimental study and DFT, Simul., J. Mater. Sci. Technol. 91 (2021) 160–167, https://doi.org/10.1016/j.jmst.2021.01.093.
[99] F. Zhang, Y. Zhu, C. Tang, Y. Chen, B. Qian, Z. Hu, Y. Chang, C. Pao, Q. Lin, S. A. Kazemi, Y. Wang, L. Zhang, X. Zhang, H. Wang, High-efficiency electrosynthesis of hydrogen peroxide from oxygen reduction enabled by a tungsten single atom catalyst with unique terdentate N_1O_2 coordination, Adv. Funct. Mater. 32 (2022) 2110224, https://doi.org/10.1002/adfm.202110224.
[100] G. Gao, Y. Jiao, E.R. Waclawik, A. Du, Single atom (Pd/Pt) supported on graphitic carbon nitride as an efficient photocatalyst for visible-light reduction of carbon dioxide, J. Am. Chem. Soc. 138 (2016) 6292–6297, https://doi.org/10.1021/jacs.6b02692.
[101] C. Deng, R. He, W. Shen, M. Li, T. Zhang, A single-atom catalyst of cobalt supported on a defective two-dimensional boron nitride material as a promising electrocatalyst for the oxygen reduction reaction: a DFT study, Phys. Chem. Chem. Phys. 21 (2019) 6900–6907, https://doi.org/10.1039/C9CP00452A.
[102] S. Yang, D.Y. Chung, Y.-J. Tak, J. Kim, H. Han, J.-S. Yu, A. Soon, Y.-E. Sung, H. Lee, Electronic structure modification of platinum on titanium nitride resulting in enhanced catalytic activity and durability for oxygen reduction and formic acid oxidation, Appl. Catal. B Environ. 174–175 (2015) 35–42, https://doi.org/10.1016/j.apcatb.2015.02.033.
[103] F. Cárdenas-Lizana, S. Gómez-Quero, N. Perret, M.A. Keane, Gold catalysis at the gas–solid interface: role of the support in determining activity and selectivity in the hydrogenation of m-dinitrobenzene, Catal. Sci. Technol. 1 (2011) 652, https://doi.org/10.1039/c1cy00051a.
[104] X. Lu, D. Wang, K.-H. Wu, X. Guo, W. Qi, Oxygen reduction to hydrogen peroxide on oxidized nanocarbon: Identification and quantification of active sites, J. Colloid Interface Sci. 573 (2020) 376–383, https://doi.org/10.1016/j.jcis.2020.04.030.
[105] Y. Hu, J. Zhang, T. Shen, Z. Li, K. Chen, Y. Lu, J. Zhang, D. Wang, Efficient electrochemical production of H_2O_2 on hollow N-doped carbon nanospheres with abundant micropores, ACS Appl. Mater. Interfaces 13 (2021) 29551–29557, https://doi.org/10.1021/acsami.1c05353.
[106] D. San Roman, D. Krishnamurthy, R. Garg, H. Hafiz, M. Lamparski, N.T. Nuhfer, V. Meunier, V. Viswanathan, T. Cohen-Karni, Engineering three-dimensional (3D) out-of-plane graphene edge sites for highly selective two-electron oxygen reduction electrocatalysis, ACS Catal. 10 (2020) 1993–2008, https://doi.org/10.1021/acscatal.9b03919.
[107] P.-C. Shi, D.-H. Si, M.-S. Yao, T.-T. Liu, Y.-B. Huang, T. Zhang, R. Cao, Spiral effect of helical carbon nanorods boosting electrocatalysis of oxygen reduction reaction, Sci. China Mater. 65 (2022) 1531–1538, https://doi.org/10.1007/s40843-021-1919-5.
[108] D. Liu, A. Barbar, T. Najam, M.S. Javed, J. Shen, P. Tsiakaras, X. Cai, Single noble metal atoms doped 2D materials for catalysis, Appl. Catal. B Environ. 297 (2021), 120389, https://doi.org/10.1016/j.apcatb.2021.120389.
[109] W. Niu, J. He, B. Gu, M. Liu, Y. Chueh, Opportunities and challenges in precise synthesis of transition metal single-atom supported by 2D materials as catalysts toward oxygen reduction reaction, Adv. Funct. Mater. 31 (2021) 2103558, https://doi.org/10.1002/adfm.202103558.
[110] Y. Wang, F.-L. Hu, Y. Mi, C. Yan, S. Zhao, Single-metal-atom catalysts: an emerging platform for electrocatalytic oxygen reduction, Chem. Eng. J. 406 (2021), 127135, https://doi.org/10.1016/j.cej.2020.127135.
[111] X. Lyu, X. Gu, G. Li, H. Chen, H. Hou, J. Hu, Hierarchical porous carbon anchored atomic/clustered cobalt for boosting oxygen reduction electrocatalysis, ChemCatChem 14 (2022), https://doi.org/10.1002/cctc.202201192.
[112] K. Liu, G. Wu, G. Wang, Role of local carbon structure surrounding FeN_4 sites in boosting the catalytic activity for oxygen reduction, J. Phys. Chem. C. 121 (2017) 11319–11324, https://doi.org/10.1021/acs.jpcc.7b00913.
[113] X. Liang, D. Wang, Z. Zhao, T. Li, Y. Gao, C. Hu, Coordination number dependent catalytic activity of single-atom cobalt catalysts for Fenton-like reaction, Adv. Funct. Mater. (2022) 2203001, https://doi.org/10.1002/adfm.202203001.
[114] X. Zhang, P. Ma, C. Wang, L. Gan, X. Chen, P. Zhang, Y. Wang, H. Li, L. Wang, X. Zhou, K. Zheng, Unraveling the dual defect sites in graphite carbon nitride for ultra-high photocatalytic H_2O_2 evolution, Energy Environ. Sci. 15 (2022) 830–842, https://doi.org/10.1039/D1EE02369A.
[115] G.-L. Chai, Z.-X. Guo, Highly effective sites and selectivity of nitrogen-doped graphene/CNT catalysts for CO_2 electrochemical reduction, Chem. Sci. 7 (2016) 1268–1275, https://doi.org/10.1039/C5SC03695J.
[116] V. Eckert, E. Haubold, S. Oswald, S. Michel, C. Bellmann, P. Potapov, D. Wolf, S. Hampel, B. Büchner, M. Mertig, A. Leonhardt, Investigation of the surface properties of different highly aligned N-MWCNT carpets, Carbon 141 (2019) 99–106, https://doi.org/10.1016/j.carbon.2018.09.035.
[117] G.-L. Chai, Z. Hou, D.-J. Shu, T. Ikeda, K. Terakura, Active sites and mechanisms for oxygen reduction reaction on nitrogen-doped carbon alloy catalysts: stone-wales defect and curvature effect, J. Am. Chem. Soc. 136 (2014) 13629–13640, https://doi.org/10.1021/ja502646c.
[118] G. Han, X. Zhang, W. Liu, Q. Zhang, Z. Wang, J. Cheng, T. Yao, L. Gu, C. Du, Y. Gao, G. Yin, Substrate strain tunes operando geometric distortion and oxygen reduction activity of CuN_2C_2 single-atom sites, Nat. Commun. 12 (2021) 6335, https://doi.org/10.1038/s41467-021-26747-1.
[119] E. Watanabe, H. Ushiyama, K. Yamashita, Theoretical studies on the mechanism of oxygen reduction reaction on clean and O-substituted Ta_3N_5 (100) surfaces, Catal. Sci. Technol. 5 (2015) 2769–2776, https://doi.org/10.1039/C5CY00088B.
[120] S. Back, S. Siahrostami, Noble metal supported hexagonal boron nitride for the oxygen reduction reaction: a DFT study, Nanoscale Adv. 1 (2019) 132–139, https://doi.org/10.1039/C8NA00059J.
[121] K. Hu, X. Wang, Y. Hu, H. Hu, X. Lin, K.M. Reddy, M. Luo, H.-J. Qiu, X. Lin, Simultaneous improvement of oxygen reduction and catalyst anchoring via multiple dopants on mesoporous carbon frameworks for flexible Al-Air batteries, ACS Nano 16 (2022) 19165–19173, https://doi.org/10.1021/acsnano.2c08332.
[122] T. Lozano, R.B. Rankin, Computational predictive design for metal-decorated-graphene size-specific subnanometer to nanometer ORR catalysts, Catal. Today 312 (2018) 105–117, https://doi.org/10.1016/j.cattod.2018.04.013.
[123] C.H. Choi, H.C. Kwon, S. Yook, H. Shin, H. Kim, M. Choi, Hydrogen peroxide synthesis via enhanced two-electron oxygen reduction pathway on carbon-coated Pt surface, J. Phys. Chem. C. 118 (2014) 30063–30070, https://doi.org/10.1021/jp5113894.
[124] H. Xu, D. Cheng, D. Cao, X.C. Zeng, A universal principle for a rational design of single-atom electrocatalysts, Nat. Catal. 1 (2018) 339–348, https://doi.org/10.1038/s41929-018-0063-z.
[125] Z. Xu, Z. Ma, K. Dong, J. Liang, L. Zhang, Y. Luo, Q. Liu, J. You, Z. Feng, D. Ma, Y. Wang, X. Sun, Electrocatalytic two-electron oxygen reduction over nitrogen doped hollow carbon nanospheres, Chem. Commun. 58 (2022) 5025–5028, https://doi.org/10.1039/D2CC01238C.
[126] K. Okaya, H. Yano, K. Kakinuma, M. Watanabe, H. Uchida, Temperature dependence of oxygen reduction reaction activity at stabilized Pt skin-PtCo alloy/graphitized carbon black catalysts prepared by a modified nanocapsule method, ACS Appl. Mater. Interfaces 4 (2012) 6982–6991, https://doi.org/10.1021/am302224n.
[127] A. Parra-Puerto, K.L. Ng, K. Fahy, A.E. Goode, M.P. Ryan, A. Kucernak, Supported transition metal phosphides: activity survey for HER, ORR, OER, and corrosion resistance in acid and alkaline electrolytes, ACS Catal. 9 (2019) 11515–11529, https://doi.org/10.1021/acscatal.9b03359.
[128] K. Kumar, T. Asset, X. Li, Y. Liu, X. Yan, Y. Chen, M. Mermoux, X. Pan, P. Atanassov, F. Maillard, L. Dubau, Fe-N-C electrocatalysts' durability: effects of single atoms' mobility and clustering, ACS Catal. 11 (2021) 484–494, https://doi.org/10.1021/acscatal.0c04625.
[129] H. Xu, X. Lv, H. Wang, J. Ye, J. Yuan, Y. Wang, Z. Zhou, S. Sun, Impact of pore structure on two-electron oxygen reduction reaction in nitrogen-doped carbon materials: rotating ring-disk electrode vs. flow cell, ChemSusChem 15 (2022), https://doi.org/10.1002/cssc.202102587.

[130] C.H. Choi, H.-K. Lim, M.W. Chung, G. Chon, N. Ranjbar Sahraie, A. Altin, M.-T. Sougrati, L. Stievano, H.S. Oh, E.S. Park, F. Luo, P. Strasser, G. Dražić, K.J. J. Mayrhofer, H. Kim, F. Jaouen, The achilles' heel of iron-based catalysts during oxygen reduction in an acidic medium, Energy Environ. Sci. 11 (2018) 3176–3182, https://doi.org/10.1039/C8EE01855C.

[131] A. Han, B. Wang, A. Kumar, Y. Qin, J. Jin, X. Wang, C. Yang, B. Dong, Y. Jia, J. Liu, X. Sun, Recent advances for MOF-derived carbon-supported single-atom catalysts, Small Methods 3 (2019) 1800471, https://doi.org/10.1002/smtd.201800471.

[132] S. Jimenez-Villegas, S.R. Kelly, S. Siahrostami, SnO_2-supported single metal atoms: a bifunctional catalyst for the electrochemical synthesis of H_2O_2, J. Mater. Chem. A 10 (2022) 6115–6121, https://doi.org/10.1039/D1TA07562D.

[133] S. Maass, F. Finsterwalder, G. Frank, R. Hartmann, C. Merten, Carbon support oxidation in PEM fuel cell cathodes, J. Power Sources 176 (2008) 444–451, https://doi.org/10.1016/j.jpowsour.2007.08.053.

[134] D. He, L. Zhong, S. Gan, J. Xie, W. Wang, Z. Liu, W. Guo, X. Yang, L. Niu, Hydrogen peroxide electrosynthesis via regulating the oxygen reduction reaction pathway on Pt noble metal with ion poisoning, Electrochim. Acta 371 (2021), 137721, https://doi.org/10.1016/j.electacta.2021.137721.

[135] A. Friedman, N. Reddy Samala, H.C. Honig, M. Tasior, D.T. Gryko, L. Elbaz, I. Grinberg, Control of molecular catalysts for oxygen reduction by variation of pH and functional groups, ChemSusChem 14 (2021) 1886–1892, https://doi.org/10.1002/cssc.202002756.

[136] J. Xi, S. Yang, L. Silvioli, S. Cao, P. Liu, Q. Chen, Y. Zhao, H. Sun, J.N. Hansen, J.-P.B. Haraldsted, J. Kibsgaard, J. Rossmeisl, S. Bals, S. Wang, I. Chorkendorff, Highly active, selective, and stable Pd single-atom catalyst anchored on N-doped hollow carbon sphere for electrochemical H_2O_2 synthesis under acidic conditions, J. Catal. 393 (2021) 313–323, https://doi.org/10.1016/j.jcat.2020.11.020.

[137] E. Luo, H. Zhang, X. Wang, L. Gao, L. Gong, T. Zhao, Z. Jin, J. Ge, Z. Jiang, C. Liu, W. Xing, Single-atom Cr-N_4 sites designed for durable oxygen reduction catalysis in acid media, Angew. Chem. Int. Ed. 58 (2019) 12469–12475, https://doi.org/10.1002/anie.201906289.

[138] S. Ding, Z. Lyu, E. Sarnello, M. Xu, L. Fang, H. Tian, S.E. Karcher, T. Li, X. Pan, J. McCloy, G. Ding, Q. Zhang, Q. Shi, D. Du, J.-C. Li, X. Zhang, Y. Lin, A MnO_x enhanced atomically dispersed iron-nitrogen-carbon catalyst for the oxygen reduction reaction, J. Mater. Chem. A 10 (2022) 5981–5989, https://doi.org/10.1039/D1TA07219F.

[139] J. Wang, Z. Li, Y. Wu, Y. Li, Fabrication of single-atom catalysts with precise structure and high metal loading, Adv. Mater. 30 (2018) 1801649, https://doi.org/10.1002/adma.201801649.

[140] J. Zhang, X. Wu, W.-C. Cheong, W. Chen, R. Lin, J. Li, L. Zheng, W. Yan, L. Gu, C. Chen, Q. Peng, D. Wang, Y. Li, Cation vacancy stabilization of single-atomic-site $Pt_1/Ni(OH)_x$ catalyst for diboration of alkynes and alkenes, Nat. Commun. 9 (2018) 1002, https://doi.org/10.1038/s41467-018-03380-z.